



## An efficient Harris hawks-inspired image segmentation method

Erick Rodríguez-Esparza<sup>a</sup>, Laura A. Zanella-Calzada<sup>b</sup>, Diego Oliva<sup>a,\*</sup>, Ali Asghar Heidari<sup>c,d</sup>, Daniel Zaldivar<sup>a</sup>, Marco Pérez-Cisneros<sup>a,\*</sup>, Loke Kok Foong<sup>e,f,\*</sup>

<sup>a</sup> División de Electrónica y Computación, Universidad de Guadalajara, CUCEI, Av. Revolución 1500, Guadalajara, Jal., Mexico

<sup>b</sup> LORIA, Université de Lorraine, Campus Scientifique BP 239, Nancy 54506, France

<sup>c</sup> School of Surveying and Geospatial Engineering, College of Engineering, University of Tehran, Tehran, Iran

<sup>d</sup> Department of Computer Science, School of Computing, National University of Singapore, Singapore, Singapore

<sup>e</sup> Institute of Research and Development, Duy Tan University, Da Nang, 550000, Vietnam

<sup>f</sup> Faculty of Civil Engineering, Duy Tan University, Da Nang 550000, Vietnam

### ARTICLE INFO

#### Article history:

Received 13 October 2019

Revised 9 March 2020

Accepted 1 April 2020

Available online 7 April 2020

#### Keywords:

Multilevel thresholding

Digital mammograms

Harris hawks optimization

Metaheuristics

Minimum cross entropy

### ABSTRACT

Segmentation is a crucial phase in image processing because it simplifies the representation of an image and facilitates its analysis. The multilevel thresholding method is more efficient for segmenting digital mammograms compared to the classic bi-level thresholding since it uses a higher number of intensities to represent different regions in the image. In the literature, there are different techniques for multilevel segmentation; however, most of these approaches do not obtain good segmented images. In addition, they are computationally expensive. Recently, statistical criteria such as Otsu, Kapur, and cross-entropy have been utilized in combination with evolutionary and swarm-based strategies to investigate the optimal threshold values for multilevel segmentation. In this paper, an efficient methodology for multilevel segmentation is proposed using the Harris Hawks Optimization (HHO) algorithm and the minimum cross-entropy as a fitness function. To substantiate the results and effectiveness of the HHO-based method, it has been tested over a benchmark set of reference images, with the Berkeley segmentation database, and with medical images of digital mammography. The proposed HHO-based solver is verified based on other comparable optimizers and two machine learning algorithms K-means and the Fuzzy IterAg. The comparisons were performed based on three groups. This first one is to provide evidence of the optimization capabilities of the HHO using the Wilcoxon test, and the second is to verify segmented image quality using the PSNR, SSIM, and FSIM metrics. Then, the third way is to verify the segmented image comparing it with the ground-truth through the metrics PRI, GCE, and Vol. The experimental results, which are validated by statistical analysis, show that the introduced method produces efficient and reliable results in terms of quality, consistency, and accuracy in comparison with the other methods. This HHO-based method presents an improvement over other segmentation approaches that are currently used in the literature.

© 2020 Elsevier Ltd. All rights reserved.

### 1. Introduction

Image segmentation is an essential preprocessing step in computer vision, pattern recognition, and image processing in various fields of applications such as medical images (Oliva et al., 2017a; Shapiro & Stockman, 2001). Basically, image segmentation is the

process of dividing an image into several non-overlapping regions or structures of interest based on grayscale, color, texture, shape, size, or position of image (Elaziz & Lu, 2019; Lalaoui, Mohamadi, & Djaalab, 2015). Otsu implements an instance of gray level quantization as segmentation because it established that the threshold that offers the best separation of classes into gray levels would be the best threshold by minimizing the sum of class variations weighted by probability (Pal & Pal, 1993; Vertan, Florea, Florea, & Badea, 2017). For this reason, the image quantization could be interpreted as image segmentation. However, in most of the works in the related literature, quantization is related to RGB images and compression (Khaled, Abdel-Kader, & Yasein, 2016; Ponti, Nazaré, & Thumé, 2016).

\* Corresponding authors at: Universidad de Guadalajara and Duy Tan University  
 E-mail addresses: erick.rodrigueze@alumno.udg.mx (E. Rodríguez-Esparza), laura.zanella-calzada@univ-lorraine.fr (L.A. Zanella-Calzada), diego.oliva@cucei.udg.mx (D. Oliva), as\_heidari@ut.ac.ir, aliasghar68@gmail.com, aliasgha@comp.nus.edu.sg, t0917038@u.nus.edu (A.A. Heidari), daniel.zaldivar@cucei.udg.mx (D. Zaldivar), marco.perez@cucei.udg.mx (M. Pérez-Cisneros), lokekokofoong@duytan.edu.vn, lokekokofoong@duytan.edu.vn (L.K. Foong).

In the literature, there exist four common types of image segmentation approaches, which can be divided into (1) clustering-based methods, (2) region based split and merging methods, (3) texture analysis based methods, and (4) histogram thresholding based methods (He & Huang, 2017). Although in recent years, the number of works in which artificial neural networks (ANN) are used as a type of method to segment images has increased to obtain a semantic segmentation (Chen, Papandreou, Kokkinos, Murphy, & Yuille, 2017; Mohammadimaneesh, Salehi, Mahdianpari, Gill, & Molinier, 2019; Panagiotakis, Grinias, & Tziritas, 2011).

One of the most widespread techniques for image segmentation is the histogram thresholding, which is widely used due to its simplicity, high accuracy, and robustness against the other methods (Ghamisi, Couceiro, & Benediktsson, 2012a). It extracts the data of the histogram from an image and defines the optimal threshold values ( $th$ ) to classify the pixels in different regions. Image thresholding techniques can be classified into two different types: bilevel and multilevel. If the objects of interest are clearly distinguished from the background of an image by a single threshold value, it is termed as bilevel thresholding, while dividing an image into several different regions by multiple threshold values is known as a multilevel threshold (MTH) (Elaziz, Ewees, & Hassanien, 2017). Regarding the implementations, MTH is more accurate than the classic bi-level threshold method for the segmentation of digital mammograms due to its diverse number of intensities used to represent regions in the image (Kumar, Kumar, Bajaj, & Singh, 2018). Mammograms help in the medical diagnosis of breast cancer, and their interpretation depends directly on the experience and skills of the radiologist. Therefore, computer-assisted diagnostic (CADx) tools have begun to be developed to improve the detection and diagnosis of this disease. The good performance of CADx tools depends on the multilevel segmentation of the image, which is the primary phase in the processing of these devices (Avuti, Bajaj, Kumar, & Singh, 2019).

To find the optimal threshold values ( $th$ ) in the MTH segmentation, there are two types of approaches: parametric and non-parametric. A parametric approach considers that each class of the image can be defined by using probability density distributions, such classes all together define the pixels contained in an image. This methodology is computationally expensive and for different classes, the statistical parameters are estimations that depend to a great extent on the initial conditions. However, the non-parametric techniques use discriminated rules to separate the pixels into homogeneous regions, then the threshold values are determined by a statistical criterion (entropy or variance) (Oliva et al., 2017b). Throughout the years there have been numerous works in the literature where some of these criteria are proposed. In 1979, Otsu (1979) presented the maximization of the variance between classes to obtain the optimal threshold values. Kapur, Sahoo, and Wong (1985) used the entropy of the histogram as a formula to find the optimal threshold values. Li and Lee (1993) submitted the minimum cross entropy method, it is used to minimizing the cross entropy between the original image and its segmented image to find the optimal thresholds. Nevertheless, these approaches have some limitations such as these exact methods are often computationally expensive, especially when the number of thresholds is increased. For this reason, the use of metaheuristics inspired by nature has attracted attention in the field of multilevel thresholding in digital images. Regarding the use of metaheuristic algorithms (MA), in past years, stochastic optimization techniques have been widely used to determine the optimal or at least near-optimal solutions for many problems faced in real life (Shen et al., 2016; Wang et al., 2017; Wang & Chen, 2020; Xu & Chen, 2014)(Qiao, Huang, Azimi, Han, 2019a). In many real applications, we need accurate analytical methods or some partially accurate alternative models, such as stochastic optimizers, to find any feasible solu-

tion or best solutions (Liu, Zhang, Chen, Jiang, Wu, Fan, Li, 2020b). These problems often have complicated, multimodal search spaces that make them hard to be solved using traditional methods that use gradient information (Jinlong et al., 2020; Xu et al., 2019; X. Zhao et al., 2014, 2019; X. Zhao, Li, Yang, Ma, & Zhu, 2014). A simple structure that can be mainly revised, efficient mechanisms to escape from local optima, and flexibility of implementation are some features of nature-inspired optimizers compared to prior methods (Chen, Yang, Heidari, & Zhao, 2019b; Faris et al., 2020; Zhang et al., 2020). As seen from literature, nature has inspired many researchers to mimic the best action in the environment and try to develop an iterative mathematical model for tackling different problems (Chen, Heidari, Zhao, Zhang, & Chen, 2020a; Chen et al., 2019a; 2020c). The key feature of all these methods is their derivative-free processes that can augment the quality of previous solutions based on some exploratory and exploitative inclinations (Faris et al., 2018; Luo et al., 2019; Mafarja et al., 2018; Xu et al., 2019).

The MA can be seen under two main perspectives, with similarities and differences in both concepts and operators (Aljarah, Mafarja, Heidari, Faris, & Mirjalili, 2020; Faris et al., 2019; Huang et al., 2020; Tang et al., 2020). The foundation of the field is constructed based on evolutionary procedures in nature (Xu et al., 2020; Zhang et al., 2020; Zhu et al., 2020). In this class, mechanisms such as mutation and crossover try to mimic the natural way of creating children from parents. The historic methods in this category are genetic algorithm (GA) developed by Holland (1992) and differential evolution (DE) proposed by Storn and Price (1997). The other group contains optimizers that iteratively update the position of agents as a swarm with simple randomized linear updating equations. The most well-regarded method in this class is the particle swarm optimizer (PSO) invented by Eberhart and Kennedy (1995). The successful optimizers are listed in Table 1.

As mentioned before, the use of MA in image thresholding allows reducing the computational effort required to find the best configuration of thresholds. In the related literature, it is possible to find several applications of MA. A new review of MA in thresholding is presented in (Pare, Kumar, Singh, & Bajaj, 2019b). Zhou, Tian, Zhao, and Zhao (2015) proposed an algorithm that combines the FFO algorithm to maximize the statistical criteria of Otsu's variance to solve the problems of time-consuming and low accuracy in image segmentation. Recently, Mousavirad and Ebrahimpour-Komleh (2019) proposed the use of the Human Mental Search Algorithm (HMSA) for image segmentation considering the Otsu's and Kapur's functions. In the same way, Resma and Nair (2018) also proposed the Krill Herd Optimization (KHO) algorithm for multilevel thresholding using the same methods that the HMSA. The Rényi's entropy was used in Pare, Bhandari, Kumar, and Singh (2019a) as a criterion for select the best thresholds using the Bat Algorithm (BA) in color images. Ahmadi, Kazemi, Aarabi, Niknam, and Helfroush (2019) introduced the Bird Mating Optimization (BMO) as an alternative for searching the thresholds in image segmentation helped by Otsu and Kapur methods. Meanwhile, Liang, Jia, Xing, Ma, and Peng (2019) proposed the use of GOA with the Tsallis entropy for multilevel image segmentation. All those techniques are examples of the extension of MA in the field of image processing, especially in the task of thresholding. In general, they provide good results, but considering the No Free Lunch (NFL) theorem introduced by Wolpert, Macready et al. (1997), not all the algorithms can solve a specific problem accurately. For that reason, it is necessary to test optimization methods.

This article introduces the HHO algorithm as an alternative method for multilevel image thresholding. The HHO algorithm is a swarm-based method proposed by Heidari et al. (2019) to handle continuous optimization tasks. This method develops new ex-

**Table 1**

List of main optimizers based on their operators.

Category	Algorithms	Developer(s)
Evolutionary	Genetic Algorithm (GA) Genetic programming (GP) Differential Evolution (DE)	Holland (1992) Koza and Koza (1992) Storn and Price (1997)
Swarm-intelligence	Particle Swarm Optimization (PSO) Ant Colony optimization (ACO) Grey Wolf Optimizer (GWO) Grasshopper Optimization Algorithm (GOA) Firefly Optimization (FFO) Teaching Learning Based Optimization (TLBO) Artificial Bee Colony (ABC) Whale Optimization Algorithm (WOA) Grasshopper Optimization Algorithm (GOA) Salp Swarm Algorithm (SSA) Harris Hawks Optimization (HHO) Gravitational Search Algorithm (GSA) Central Force Optimization (CFO) Harmony Search Algorithm (HS) Sine-Cosine Algorithm (SCA) Slime Mould Algorithm (SMA)	Eberhart and Kennedy (1995) Dorigo and Di Caro (1999) Mirjalili, Mirjalili, and Lewis (2014) Saremi, Mirjalili, and Lewis (2017) Yang (2010) Rao, Savsani, and Vakharia (2011) Karaboga and Basturk (2007) Mirjalili and Lewis (2016) Saremi et al. (2017) Mirjalili et al. (2017) Heidari et al. (2019) Rashedi, Nezamabadi-Pour, and Saryazdi (2009) Formato (2007) Geem et al. (2001) Mirjalili (2016) Li, Chen, Wang, Heidari, and Mirjalili (2020)

ploratory and exploitative trends in the field based on the simulation of hawks and rabbits. The results initially presented reveal that the HHO is among the efficient methods proposed recently, and the solutions are of high quality. The HHO is selected due it has not been tested over real problems like image segmentation. Moreover, its use permits to handle with the drawback of MTH avoiding to fail in sub-optimal values. MTH then is a multidimensional problem that increases its complexity with the amount of *th* values. Considering the above, the aim is to present an alternative efficient multilevel thresholding approach based on the HHO for digital images. Since HHO is new, it has not been extensively used or tested in many implementations. Finally, to verify the flexibility of the proposed MTH method based on HHO, it has been used to segment digital mammograms.

The motivation of this paper then is related to two directions. The first is to test the HHO in an image processing application. Meanwhile, the second direction is to use the segmentation proposal on a real problem related to medical images. Considering such motivations, we develop an efficient tool that can be used as a preprocessing step in different image processing systems. The proposed approach is called MCET-HHO, where the HHO algorithm is used to find the best configuration of thresholds that segment an image by considering the Minimum Cross Entropy Thresholding (MCET) as a fitness function. In the HHO, each solution is a set of thresholds that is part of a population. Using the operators that mimics the behavior of Harris hawks, the algorithm evolves the solutions until finding the optimal. At the end of the iterative process, the best solution is selected and applied to segment an image. The quality of the results is weighed using different metrics as the Peak Signal-to-Noise Ration (PSNR) (Hore & Ziou, 2010), Feature Similarity (FSIM) index (Zhang, Zhang, Mou, & Zhang, 2011) and Structural Similarity (SSIM) index (Wang, Bovik, Sheikh, Simoncelli et al., 2004). Moreover, the results obtained by the proposed approach are compared to validate the performance. For the comparisons, they are both metaheuristic approaches and machine learning methods. The idea is to provide evidence about the performance of HHO with different segmentation techniques. For the MA, they have been considered methods as the PSO, DE, FFO, ABC, HS, and SCA. Such algorithms were taken based on their applications an trying to cover from the classical to the most recent proposals. Meanwhile, the K-means (Saha & Hossain, 2017) algorithm, and the fuzzy method with an iterative average aggregation (IterAg) (Aja-Fernández, Curiale, & Vegas-Sánchez-Ferrero, 2015) have been used as non-MA. The K-means is a clustering-based approach

that works directly with the pixel, and the fuzzy-based technique considers the histogram to generate the thresholds. The comparisons were performed by different statistical and non-parametric analysis to validate that the solutions provided by the HHO are competitive.

The main contributions of this article can be summarized in the following points:

- Substantiating the HHO in dealing with a real multidimensional application related to image processing.
- Proposing an efficient method for multilevel thresholding by using the minimum cross-entropy.
- Applying the proposed technique to the segmentation of digital mammograms; this approach is utilized in CADx systems.

The remainder paper is organized as follows: Section 2 provides the basics of image segmentation and introduces the minimum cross-entropy. In Section 3, we described the HHO algorithm. Section 4 presents the proposed HHO for multilevel thresholding. Section 5 explains the materials and methods for experiments; meanwhile, in Section 6 the results are presented and discussed. Finally, in Section 7 are included some conclusions.

## 2. Image segmentation

In this section, the problem of selecting multiple thresholds in grayscale images is presented using the minimization of cross-entropy as criteria for segmentation. The key objective of image segmentation is to facilitate the processing of images. Image segmentation refers to the partition of an image into a set of regions that compose it, and it is usually performed by dividing the image histogram via selecting optimal threshold values. Finding optimal threshold levels is not an easy task because an image histogram can contain valleys and wide peaks with different heights. The cross-entropy method can solve these problems by measuring the homogeneity of the histogram information between the original image and its segmented image.

### 2.1. Minimum cross entropy method

In 1968, Kullback (1968) proposed the cross entropy under the name of directed divergence. The cross entropy measures the information theoretic distance between the two probability distribu-

tions,  $\mathbf{P}=\{p_1, p_2, \dots, p_N\}$  and  $\mathbf{Q}=\{q_1, q_2, \dots, q_N\}$  defined by:

$$D(\mathbf{P}, \mathbf{Q}) = \sum_{i=1}^N p_i \log \frac{p_i}{q_i} \quad (1)$$

This can be seen as a branch of the maximum entropy method by establishing equal initial estimates for all  $p_i$  when there is no prior information.

The MCET-HHO algorithm selects the optimal threshold value by minimizing the cross-entropy between the original image and the thresholded image. A lower value of the cross-entropy represents less uncertainty and greater homogeneity. Let  $\mathbf{I}$  be the original image and  $h(i), i = 1, 2, \dots, L$  be the corresponding histogram with  $L$  being the number of gray levels. The thresholded image ( $\mathbf{I}_{th}$ ) is constructed using the threshold value ( $th$ ) by:

$$\mathbf{I}_{th}(x, y) = \begin{cases} \mu(1, th), & \text{if } \mathbf{I}(x, y) < th \\ \mu(th, L+1), & \text{if } \mathbf{I}(x, y) \geq th \end{cases} \quad (2)$$

where

$$\mu(a, b) = \sum_{i=a}^{b-1} ih(i) / \sum_{i=a}^{b-1} h(i) \quad (3)$$

The cross entropy is calculated from rewriting Eq. (2) to obtain an entropy value as an objective function (also called fitness) by:

$$f_{cross}(th) = \sum_{i=1}^{th-1} ih(i) \log \left( \frac{i}{\mu(1, th)} \right) + \sum_{i=th}^L ih(i) \log \left( \frac{i}{\mu(th, L+1)} \right) \quad (4)$$

This objective function considers a threshold value for bilevel thresholding, the Eq. (4) can be extended to a multilevel approach. However, it can be computationally expensive. To reduce this shortcoming, Yin (2007) proposed a faster recursive programming technique to obtain the optimal threshold for digital images. Then, the Eq. (4) can be expressed as:

$$f_{cross}(th) = \sum_{i=1}^L ih(i) \log(i) - \sum_{i=1}^{th-1} ih(i) \log(\mu(1, th)) - \sum_{i=th}^L ih(i) \log(\mu(th, L+1)) \quad (5)$$

The multilevel approach of Eq. (5) is based on the vector  $\mathbf{th} = [th_1, th_2, \dots, th_{nt}]$ , which contains  $nt$  different thresholds values, by:

$$f_{cross}(\mathbf{th}) = \sum_{i=1}^L ih(i) \log(i) - \sum_{i=1}^{nt} H_i \quad (6)$$

where  $nt$  is the total number of thresholds and  $H_i$  is defined as:

$$\begin{aligned} H_1 &= \sum_{i=1}^{th_1-1} ih(i) \log(\mu(1, th_1)) \\ H_k &= \sum_{i=th_{k-1}}^{th_k-1} ih(i) \log(\mu(th_{k-1}, th_k)), \quad 1 < k < nt \\ H_{nt} &= \sum_{i=th_{nt}}^L ih(i) \log(\mu(th_{nt}, L+1)) \end{aligned} \quad (7)$$

### 3. Harris hawks optimization

One of the smartest birds in natural environments is called Harris hawks. These birds know how to manage a group and cooperate intelligently for finding a targeted rabbit (Ridha, Heidari, Wang, &

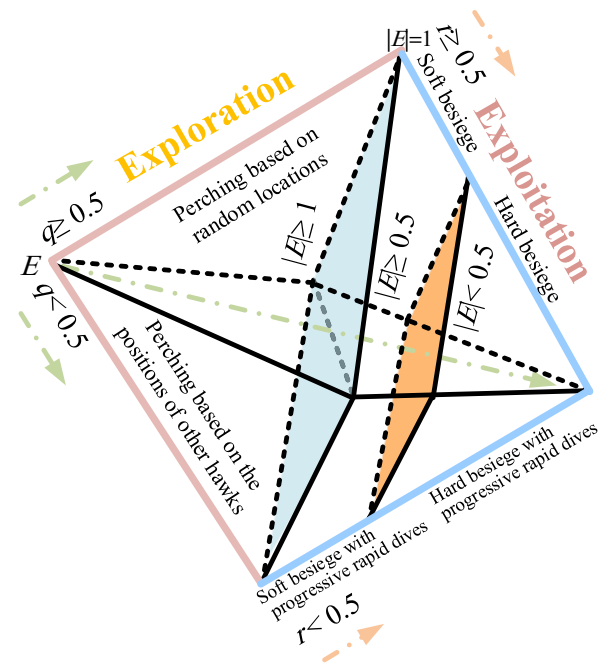


Fig. 1. Main steps of HHO based on Heidari et al. (2019).

**Table 2**  
Meaning of symbols in HHO.

Description	Symbol
Position of agents, $i$ th element	$\mathbf{X}, X_i$
Best agent	$X_{rabbit}$
Random agent	$X_{rand}$
Average agent	$X_m$
Swarm size, iteration counter, maximum number of iterations	$N, t, T$
Random values inside (0,1)	$r_1, r_2, r_3, r_4, r_5, q$
Dimension, upper and lower limits of variables	$D, LB, UB$
Escaping energy, initial state of energy	$E, E_0$

Chen, 2020). Different attacking and escaping behaviors occur in this process (Chen, Jiao, Wang, Heidari, & Zhao, 2020b). In 2019, Heidari et al. (2019) proposed a method called HHO that mathematically models these interactions to tackle optimization problems. In HHO, we have a series of hawks that play the role of candidate solutions, while the best-obtained solution is called rabbit. This method employs two phases of exploration and four stages of exploitation. In the exploitation step, it utilizes hard and soft sieges to further focus on the vicinity of obtained solutions. The overall stages of HHO are vividly demonstrated in Fig. 1. Before detailed explanations of steps, we represent the meaning of symbols used in the next subsections. Table 2 shows these symbols and their definitions.

#### 3.1. Exploration phase

There are two strategies in HHO to perform the exploration phases:

$$\mathbf{X}(t+1) = \begin{cases} X_{rand}(t) - r_1 |X_{rand}(t) - 2r_2 X(t)| & q \geq 0.5 \\ (X_{rabbit}(t) - X_m(t)) - r_3 (LB + r_4 (UB - LB)) & q < 0.5 \end{cases} \quad (8)$$

where  $X_m$  is the average position of hawks obtained using Eq. (9):

$$X_m(t) = \frac{1}{N} \sum_{i=1}^N X_i(t) \quad (9)$$

### 3.2. Transition from exploration to exploitation

To change between different diversification and intensification stages of HHO, (Heidari et al., 2019) utilized a dynamic parameter within the core operations of HHO. This parameter represents the concept of energy over the course of iterations, which can be obtained using the following rule:

$$E = 2E_0 \left(1 - \frac{t}{T}\right) \quad (10)$$

where  $E_0$  is a random parameter inside (-1,1).

### 3.3. Exploitation phase

#### 3.3.1. Soft besiege

This behavior is modeled by the following rules:

$$\mathbf{X}(t+1) = \Delta\mathbf{X}(t) - E|JX_{rabbit}(t) - \mathbf{X}(t)| \quad (11)$$

$$\Delta\mathbf{X}(t) = X_{rabbit}(t) - \mathbf{X}(t) \quad (12)$$

where  $J = 2(1 - r_5)$  is the jump strength of the rabbit.

#### 3.3.2. Hard besiege

This operator is defined in Eq. (13):

$$\mathbf{X}(t+1) = X_{rabbit}(t) - E|\Delta\mathbf{X}(t)| \quad (13)$$

#### 3.3.3. Soft besiege with the progressive rapid dives (PRD)

In soft besiege stage, it is supposed that agents can decide on their next action based on the rule represented in Eq. (14):

$$Y = X_{rabbit}(t) - E|JX_{rabbit}(t) - \mathbf{X}(t)| \quad (14)$$

The LF movements are employed in this step of the HHO by applying the following rule (Thaher, Heidari, Mafarja, Dong, & Mirjalili, 2020):

$$Z = Y + S \times LF(D) \quad (15)$$

where  $S$  is a vector by size  $1 \times D$  and LF shows the levy flight function, which is computed by Eq. (16):

$$LF(x) = \frac{u \times \sigma}{|v|^{\frac{1}{\beta}}}, \sigma = \left( \frac{\Gamma(1 + \beta) \times \sin(\frac{\pi\beta}{2})}{\Gamma(\frac{1+\beta}{2}) \times \beta \times 2^{(\frac{\beta-1}{2})}} \right)^{\frac{1}{\beta}} \quad (16)$$

where  $u, v$  are values of the LF randomly defined and  $\beta$  is 1.5.

In consequence, the Eq. (17) is used in this step.

$$\mathbf{X}(t+1) = \begin{cases} Y & \text{if } F(Y) < F(X(t)) \\ Z & \text{if } F(Z) < F(X(t)) \end{cases} \quad (17)$$

where  $Y$  and  $Z$  are computed by Eqs. (14) and (15).

#### 3.3.4. Hard besiege with the PRD

This operator of the HHO is represent by the following rule:

$$\mathbf{X}(t+1) = \begin{cases} Y' & \text{if } F(Y') < F(X(t)) \\ Z' & \text{if } F(Z') < F(X(t)) \end{cases} \quad (18)$$

where  $Y'$  and  $Z'$  are computed using the Eqs. (19) and (20).

$$Y' = X_{rabbit}(t) - E|JX_{rabbit}(t) - X_m(t)| \quad (19)$$

$$Z' = Y' + S \times LF(D) \quad (20)$$

where  $X_m(t)$  is obtained using Eq. (9).

### 3.4. Pseudocode of HHO

The pseudocode of the HHO is described in Algorithm 1.

---

#### Algorithm 1 Pseudo-code of HHO algorithm.

---

```

Inputs:  $N$  and  $T$ 
Outputs:  $X_{rabbit}$ 
Initialize  $X_i (i = 1, 2, \dots, N)$ 
while (stopping condition is not met) do
    Calculate the fitness values
    Set  $X_{rabbit}$  as the best solution
    for (each hawk ( $X_i$ )) do
        Update  $E_0$  and jump strength  $J$  ▷  $E_0=2\text{rand}()-1$ ,
         $J=2(1-\text{rand}())$ 
        Update  $E$  by Equation (10)
        if ( $|E| \geq 1$ ) then ▷ Exploration phase
            Update the members of mission by Equation (8)
        if ( $|E| < 1$ ) then ▷ Exploitation phase
            if ( $r \geq 0.5$  and  $|E| \geq 0.5$ ) then ▷ Soft besiege
                Update the members of mission by Eq. (11)
            else if ( $r \geq 0.5$  and  $|E| < 0.5$ ) then ▷ Hard besiege
                Update the members of mission by Eq. (13)
            else if ( $r < 0.5$  and  $|E| \geq 0.5$ ) then ▷ Soft besiege with
                the PRD
                Update the members of mission by Eq. (17)
            else if ( $r < 0.5$  and  $|E| < 0.5$ ) then ▷ Hard besiege
                with the PRD
                Update the members of mission by Eq. (18)
        Return  $X_{rabbit}$ 

```

---

## 4. MCET-HHO

In this paper, an efficient algorithm is introduced to find the optimal threshold values for multilevel thresholding. These optimal thresholds are useful for image segmentation. Fig. 2 illustrates the flowchart of MCET-HHO. First, a grayscale image ( $\mathbf{I}_{Gr}$ ) is read, and its histogram ( $h_{Gr}$ ) is obtained. Next, the parameters of the number of Harris hawks in the population ( $N$ ), the maximum number of iterations ( $T$ ) are defined, and the number of thresholds ( $nt$ ) is set. After that, the initial position of the population is randomly generated ( $\mathbf{X}$ ), and the fitness value is calculated for each individual in the population. The positions of the hawks are sets of numbers from 0 to 255, which represent the thresholds to which the 8-bit intensity image will be segmented, and the fitness value is obtained by evaluating the thresholds in the cross-entropy function (Eq. (6)). Then, the position of the hawks with the minimum fitness value is set as  $X_{rabbit}$ , and the energy of the prey ( $E$ ) for each hawk are updated. When the stop criterion ( $t = T$ ) is satisfied, the best position found among the population of hawks is established as the threshold vector ( $\mathbf{th}$ ). Finally,  $\mathbf{I}_s$  is generated using  $\mathbf{th}$  in Eq. (21).

### 4.1. MCET-HHO Implementation

For this approach, the HHO algorithm is developed to minimize the cross-entropy. The proposed method is simple and easy to implement. We present different steps of the MCET-HHO algorithm below:

- Step 1: Read the image  $\mathbf{I}$  and conver it to grayscale  $\mathbf{I}_{Gr}$ .
- Step 2: Calculate the histogram  $h_{Gr}$  of  $\mathbf{I}_{Gr}$ .
- Step 3: Set the HHO parameters:  $T, N$ .
- Step 4: Initialize the location of a population of Harris hawks  $\mathbf{X}$  of  $N$  random particles with  $nt$  dimensions.
- Step 5: Evaluate the objective function ( $f_{cross}$ ) with Eq. (6) for each element of  $\mathbf{X}$ .
- Step 6: Set  $X_{rabbit}$  as the location of rabbit (best location).

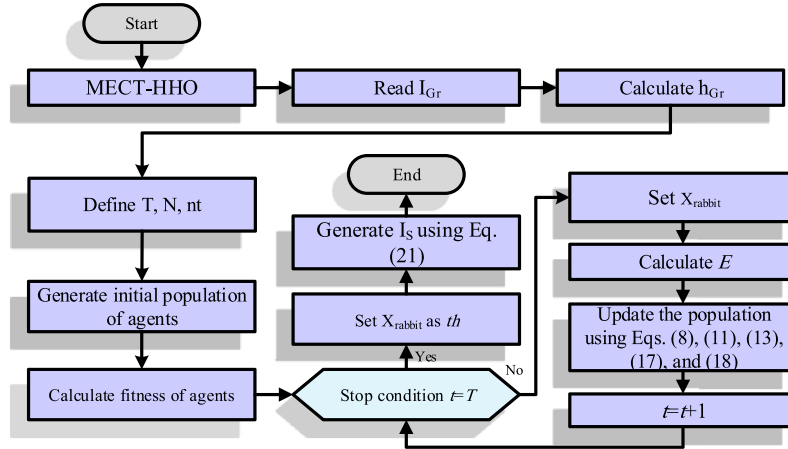


**Fig. 2.** The flowchart of MCET-HHO.

- Step 7: Calculate  $E$  with Eq. (10) for each hawk  $X_i$ .
- Step 8: Update the location of Harris hawks  $\mathbf{X}$  depending of the energy value of his prey.
- Step 9: The  $t$  index is increased in 1, if the stop criteria ( $t \geq T$ ) are not satisfied jump to step 5.
- Step 10: Generate the segmented image  $I_s$  with the thresholds values contained in  $X_{rabbit}$ , using the Eq. (21).

#### 4.2. Multilevel thresholding

The segmentation of the unique image is achieved by using the optimal thresholds computed by the HHO; they should adequately minimize the objective function. An easy rule widely used to segment the image with the thresholds, which is defined as follows (Hinojosa, Oliva, Cuevas, Pérez-Cisneros, & Pájares, 2018):

$$I_s(x, y) = \begin{cases} 0, & \text{if } I_{Gr}(x, y) < th_1 \\ th_{i-1}, & \text{if } th_{i-1} \leq I_{Gr}(x, y) < th_i, \quad i = 2, 3, \dots, nt - 1 \\ th_{nt}, & \text{if } I_{Gr}(x, y) \geq th_{nt} \end{cases} \quad (21)$$

where  $I_s$  is the segmented image,  $I_{Gr}$  is the original image in grayscale and  $th_i$  are the optimal threshold values used to segment the image.

#### 4.3. Computational complexity

The computational complexity of the MCET-HHO depends mainly on two processes: the evaluation of the cross-entropy function and the operation of the HHO algorithm. The computational cost of the evaluation of the cross-entropy function is  $O(nt * XY)$ , where  $nt$  is the number of thresholds and  $XY$  is the number of pixels, while for the operation of the HHO algorithm is  $O(T * N * D)$ ,  $T$  is the maximum number of iterations,  $N$  is the number of hawks, and  $D$  is the dimension of the problem (Heidari et al., 2019). Therefore, computational complexity of MCET-HHO is  $O(nt * XY * T * N)$ , as shown,  $D$  is eliminated because  $nt$  represents the same.

### 5. Materials and methods

In this section, we presented the materials required for the development of this work, as well as the methods applied based on the techniques described above.

#### 5.1. Experimental setup

Three sets of images are used to test the proposed approach. The first set is composed of benchmark images commonly used in

the image processing literature that contains 11 images with different levels of complexity, include Lena, Peppers, Cameraman, Baboon, Barbara, Bridge, Pirate, Butterfly, Jetplane, Living room, and Lake. Oliva et al. (2017b), Elaziz, Oliva, Ewees, and Xiong (2019), Agrawal, Panda, Bhuyan, and Panigrahi (2013). All images present the same size ( $512 \times 512$  pixels), except for Lena and Cameraman images, which are  $256 \times 256$  pixels. Fig. 3 shows the benchmark of images used.

The second set of images is used to compare the MCET-HHO approach against human segmentation manually performed. This set consists of 100 validation and 200 test images of the Berkeley segmentation dataset (Arbelaez, Maire, Fowlkes, & Malik, 2011), which is available at this link<sup>1</sup>.

The third set of images is used to determine the performance of the MCET-HHO applied to medical images. This set consists of eight digital mammograms obtained from the Digital Database for Screening Mammography (DDSM), which is available for public access at this link<sup>2</sup> (Heath, Bowyer, Kopans, Moore, & Kegelmeyer, 2000).

According to the related literature, the number of total thresholds selected are  $nt = 2, 3, 4, 5$  (Horng & Liou, 2011; Oliva et al., 2017b). The MA used in this work has the same conditions for a fair comparison, the stopping criterion is the maximum number of iterations ( $T$ ) and it is set to 250, which are executed 35 times ( $T_E$ ) for each image and used the same population size ( $N$ ) of 30.

For the comparisons, we considered the Particle Swarm Optimization (PSO) (Kennedy, 2010), Firefly Optimization (FFO) (Yang, 2009), Differential Evolution (DE) (Storn & Price, 1997), Harmony Search (HS) (Geem, Kim, & Loganathan, 2001), Artificial Bee Colony (ABC) (Karaboga & Basturk, 2007), and Sine-Cosine Algorithm (SCA) (Mirjalili, 2016). All these method are metaheuristic algorithms; moreover, the K-means algorithm (Saha & Hossain, 2017) and the fuzzy IterAg (Aja-Fernández et al., 2015) are also used for comparative purposes.

The parameters of each investigated method are shown in the Table 3. All the algorithms were adjusted experimentally following the references that proposed and used them (Geem et al., 2001; Karaboga & Basturk, 2007; Kennedy, 2010; Mirjalili, 2016; Storn & Price, 1997; Yang, 2009). All experiments were done using Matlab 9.4 on an Intel Core i5 CPU @ 2.7Ghz with 8 GB of RAM.

<sup>1</sup> [www2.eecs.berkeley.edu/Research/Projects/CS/vision/grouping/resources.html](http://www2.eecs.berkeley.edu/Research/Projects/CS/vision/grouping/resources.html).

<sup>2</sup> [www.eng.usf.edu/cvprg/Mammography/Database.html](http://www.eng.usf.edu/cvprg/Mammography/Database.html).

**Fig. 3.** Set of benchmark images.

**Table 3**  
Selected parameters for HHO, PSO, FFO, DE, HS, ABC and SCA.

HHO	PSO	FFO	ABC
Pop. N: 30	Pop. N: 30 Inertia Weight: 1 Damping Ratio: 0.99 Personal Lrn. Coef.: 1.5 Global Lrn. Coef.: 2	Pop. N: 30 Light Absorption Coef.: 1 Attraction Coef.: 0.2 Mutation Coef.: 0.25 Damping Ratio: 0.8	Pop. N: 30 Limit Parameter: 0.6 Damping Ratio: 1
SCA	HS	DE	
Pop. N: 30	Pop. N: 30 Nbr. of New Harmonies: 10 Consideration Rate: 0.9 Pitch Adjustment Rate: 0.1 Damping Ratio: 0.8	Pop. N: 30 LB of Scaling Factor: 0.2 UB of Scaling Factor: 0.8	Crossover Prob: 0.2

## 5.2. Metrics

Two groups of metrics are used to evaluate the performance of the MCET-HHO approach. The metrics of the first group are used for the image quality in the first and third tests, and the metrics of the second group are applied to compare the edges of the segmented image in the second test.

### 5.2.1. Metrics to evaluate the segmented image quality

Since the algorithm presented in this work is stochastic, different statistical metrics are employed that help to verify the efficiency of the optimizers. One of the most important features we seek in these methods is the stability of the optimizers in each independent test. The standard deviation (STD) presented in Eq. (22) is used to verify the stability. According to Ghamisi, Couceiro, Benediktsson, and Ferreira (2012b), if the STD value increases, the algorithm becomes more unstable.

$$STD = \sqrt{\sum_{i=1}^{T_E} \frac{\sigma_i - \mu}{T_E}} \quad (22)$$

Another metric used to evaluate quality of the segmentation is the PSNR, which is defined by the Eq. (23) (Hore & Ziou, 2010). The PSNR compares the segmented and the original images using Root Mean Square Error (RMSE) of each pixel. A higher PSNR indicates that more similarity exists between the images that are reflected in a better quality of the segmentation process.

$$PSNR = 20 \log \left( \frac{255}{RMSE} \right) \quad (23)$$

where,

$$RMSE = \sqrt{\frac{1}{MN} \sum_{i=1}^M \sum_{j=1}^N |I_{Gr}(i, j) - I_s(i, j)|^2} \quad (24)$$

where  $M, N$  define the size of the image,  $I_{Gr}$  is the original image in grayscale and  $I_s$  is the segmented image.

The Structure similarity (SSIM) index is used to analyze the internal structures in the segmented image (Wang et al., 2004), and it is defined in Eq. (25). Then, a higher SSIM value represents a better segmentation of the original image due that the structures in both images coincide.

$$SSIM = \frac{(2\mu_{I_{Gr}}\mu_{I_s} + C_1)(2\sigma_{I_{Gr}I_s} + C_2)}{(\mu_{I_{Gr}}^2 + \mu_{I_s}^2 + C_1)(\sigma_{I_{Gr}}^2 + \sigma_{I_s}^2 + C_2)} \quad (25)$$

where

$$\sigma_{I_{Gr}I_s} = \frac{1}{N-1} \sum_{i=1}^N (I_{Gr,i} + \mu_{I_{Gr}})(I_{s,i} + \mu_{I_s}) \quad (26)$$

where  $\mu_{I_{Gr}}$  and  $\mu_{I_s}$  are the mean value of the original and the segmented image, respectively. The values of  $\sigma_{I_{Gr}}$  and  $\sigma_{I_s}$  correspond

to the standard deviation.  $C_1$  and  $C_2$  are constants used to avoid the instability when  $\mu_{I_{Gr}} + \mu_{I_s} \approx 0$ . The values of  $C_1$  and  $C_2$  are set to 0.065 considering the experiments by Agrawal et al. (2013).

The last quality metric used in this paper is the Feature Similarity (FSIM) index defined in Eq. (27). The FSIM measures the similarity between the segmented and the original image in terms of their internal features (corners, borders, etc.) (Zhang et al., 2011). A higher value of FSIM is interpreted as a better performance of the thresholding method.

$$FSIM = \frac{\sum_{\omega \in \Omega} \mathbf{S}_L(\omega) \mathbf{P}\mathbf{C}_m(\omega)}{\sum_{\omega \in \Omega} \mathbf{P}\mathbf{C}_m(\omega)} \quad (27)$$

where  $\Omega$  represents the entire domain of the image, the values of  $\mathbf{S}_L$  are defined by:

$$\begin{aligned} \mathbf{S}_L(\omega) &= \mathbf{S}_{PC}(\omega) \mathbf{S}_G(\omega) \\ \mathbf{S}_{PC}(\omega) &= \frac{2PC_1(\omega)PC_2(\omega) + T_1}{PC_1^2(\omega) + PC_2^2(\omega) + T_1} \\ \mathbf{S}_G(\omega) &= \frac{2G_1(\omega)G_2(\omega) + T_2}{G_1^2(\omega) + G_2^2(\omega) + T_2} \end{aligned} \quad (28)$$

where  $T_1$  and  $T_2$  are constants and the values chosen are  $T_1 = 0.85$  and  $T_2 = 160$ . From the Eq. (28),  $G$  is the gradient magnitude of an image defined by the Eq. (29), and the phase congruence ( $PC$ ) are computed as the Eq. (30).

$$G = \sqrt{G_x^2 + G_y^2} \quad (29)$$

$$PC = \frac{E(\omega)}{(\epsilon + \sum_n A_n(\omega))} \quad (30)$$

where  $A_n(\omega)$  is the local amplitude on scale  $n$  and  $E(\omega)$  is the magnitude of the response vector in  $\omega$  on  $n$ .  $\epsilon$  is a small positive number and  $PC_m = \max(PC_1(\omega), PC_2(\omega))$ .

In order to statistically validate the numerical results, the non-parametric Wilcoxon rank-sum test is used to indicate significant differences between the behavior of one algorithm and another (Wilcoxon, 1992).

### 5.2.2. Metrics to evaluate the segmented image

The first metric to assess image segmentation is the Probability Rand Index (Unnikrishnan, Pantofaru, & Hebert, 2007) defined in Eq. (31). In this metric, the similarity between the clustering of the contours of the image segmented by the algorithm ( $S$ ) and the manual clustering obtained by the database ( $S_{Gt}$ ) is compared.

$$PRI = \frac{1}{T} \sum_{i,j} [c_{ij} p_{ij} + (1 - c_{ij})(1 - p_{ij})] \quad (31)$$

where  $c_{ij}$  is the event that pixels  $(i, j)$  of  $S$  and  $S_{Gt}$  have the same label.  $p_{ij}$  is the probability of the  $c_{ij}$ , and  $T$  is the total number of pixel pairs.

Another metric used is the Variation of Information (Vol) that defines the distance between the two segmentations ( $S$  and  $S_{Gt}$ ) as the average conditional entropy between one segmentation given the other (Yang, Wright, Ma, & Sastry, 2008), defined in the Eq. (32).

$$Vol = H(S) + H(S_{Gt}) - 2I(S, S_{Gt}) \quad (32)$$

where  $H$  represents the entropy and  $I$  the information between the clustering  $S$  and the  $S_{Gt}$ .

The last metrics used is the Global Consistency Error (GCE) by Eq. (33), that measures the degree that one segmentation can be seen as a refinement of the other or the degree of overlap of the regions (Peng, Zhang, & Zhang, 2013).

$$GCE = \frac{1}{n} \min \left\{ \sum_i E(S, S_{Gt}, p_i), \sum_i E(S_{Gt}, S, p_i) \right\} \quad (33)$$

where the local refinement ( $E$ ) is defined as:

$$E(S, S_{Gt}, p_i) = \frac{|R(S, p_i)/R(S_{Gt}, p_i)|}{|R(S, p_i)|} \quad (34)$$

$R(S, p_i)$  be the set of pixels in segmentation  $S$  that contains pixel  $p_i$ .

## 6. Results and discussion

This section provides experimental results from different aspects to evaluate the efficiency of the proposed method. One of the valid strategies to confirm the proposed models in analytical or swarm-based methods is to compare their results using a set of known samples or benchmarks (Gao, Guirao, Basavanagoud, & Wu, 2018a; Gao, Guirao, Abdel-Aty, & Xi, 2019; Gao, Wang, Dimitrov, & Wang, 2018b; Gao, Wu, Siddiqui, & Baig, 2018c; Liu, Zhang, Fan, Jiang, & Daemen, 2020c). The results of the HHO algorithm applied to the first set of benchmark images are compared with the results of PSO, DE, HS, ABC, FFO, SCA, the *K*-means algorithm, and the fuzzy IterAg. However, the results of the HHO algorithm applied to the second set of images (digital mammograms) are only compared with the *K*-means algorithm and the Fuzzy IterAg.

### 6.1. Experiments with benchmark images

The first set of images used as a benchmark for the development of this work is presented in Fig. 3, as well as their correspondent histograms, where it is possible to observe the heterogeneity in the intensities of the gray levels for the different images, allowing to test the behavior of the approach that is proposed with different data and, thus, to verify its robustness.

Table 4 presents the values of the best thresholds obtained for the levels tested, 2, 3, 4, and 5, using the different algorithms, HHO, PSO, FFO, DE, HS ABC, SCA, *K*-means and Fuzzy IterAg. In most cases, levels 2, 3, and 4 have similar values for most of the algorithms, while for level 5 some crucial differences are presented in the threshold values obtained, especially for the SCA algorithm. Also, it is notable that for most of the images, the algorithms *K*-means and Fuzzy IterAg present lower values for the first threshold of the different levels in comparison to the other algorithms, while for the rest of the thresholds in the levels, they present higher values, being more evident in the last threshold values.

In Table 5, a comparison of the average cross-entropy values and their std obtained for each level through applying the MCET-HHO algorithm and the other set of algorithms is presented, where the best values are observed in bold. For most images, the average values obtained for the HHO algorithm are the best for each level, and, for the algorithms PSO, DE, HS, and ABC, the average values

obtained for level 2 are similar to those obtained by the HHO algorithm, being the best. For the rest of the levels, there are some significant differences between the set of algorithms and the HHO.

In general, the PSO, DE, and HS algorithms present very similar results to the HHO, specifically for levels 3 and 4, as in the case of the images Cameraman and Living room. For level 5, the HHO algorithm presents the best average values for all the images, except for the Peppers and Bridge images, where their best values are obtained through the ABC and DE algorithms, respectively. The FFO and SCA present the less significant results, obtaining only one significant value the FFO, while the SCA does not obtain any significant value among its average results.

Therefore, with the exception of three values, the HHO algorithm presents the most significant average results at all levels for each image, also showing std values of zero in most cases, checking the robustness of the algorithm's behavior.

Table 6 presents the PSNR values obtained for each of the algorithms, which, as mentioned before, allows to evaluate the affinity between the segmented image and the original, where a higher value represents better quality of the thresholding. In general, the higher PSNR values are obtained using the HHO, PSO, FFO, DE, HS, and ABC algorithms, but some of the present better performance for a set of images than for others. In the case of the HHO algorithm, the mean of the PSNR obtained for the image Lena present the higher results for all the levels in comparison to the rest of the algorithms, while for the images Cameraman, Living room, Bridge and Lake present the best results in comparison with the other algorithms for at least two over the four different levels. It is important to note that for most of the images, level 2 shows a good PSNR value not only for the HHO algorithm, but for PSO, DE, HS, and ABC. In the case of the FFO algorithm, the images Baboon and Bridge obtained the higher values for all or at least three of the levels; while for the ABC algorithm, the highest values for all or at least three of the levels are present in the images Living room and Lena. In the case of the DE algorithm, the best PSNR values were obtained for all the levels in the image Bridge, while for the images Cameraman, Lena, Living room, and Lake, there were obtained significant PSNR values for at least two of the levels. On the other hand, the *K*-means and Fuzzy IterAg algorithms do not present part of the highest PSNR results in any of the images.

Therefore, the highest PSNR values are obtained through the HHO, FFO, DE, HS and ABC algorithms, presenting the best performance with the images Cameraman, Lena, Living room, Bridge and Lake, showing a good affinity between the original image and the segmented image.

Table 7 presents a comparison of the average SSIM values obtained from the behavior of the different algorithms under a cross-entropy approach. The best results are shown in bold, indicating better segmentation of the original image. As is possible to observe, the results obtained with the algorithms HHO and ABC are very similar, being significant it most of the images, especially in the Cameraman, Lena, Baboon, Pirate, Jetplane, Pepper, Living room and Lake images. On the other hand, the results obtained by the *K*-means and Fuzzy IterAg algorithms present lower values than the rest of the algorithms.

In the case of the images Barbara and Bridge, the best results are presented by the FFO algorithm, while for the butterfly image, none of the algorithms has an outstanding behavior. The results of the PSO, DE and HS algorithms are significant and very similar; however, the HHO and ABC algorithms present better values.

In Table 8 is shown a comparison of the values obtained for the FFSIM metric applying the different algorithms under a cross-entropy approach. The best values obtained are presented in bold, which represents the best quality of the segmentation, being the highest values those with the most significant performance of the thresholding method.

**Table 4**

The best thresholds values of all algorithms for levels 2, 3, 4, and 5 in the set of benchmark images.

Image	nTh	HHO	PSO	FFO	DE	HS	ABC	SCA	K-means	Fuzzy IterAg
Cameraman	2	51 137	51 137	51 137	51 137	51 137	51 137	51 137	31 155	29 160
	3	30 83 144	30 83 144	30 83 144	30 83 144	30 83 1447	30 83 144	30 84 140	23 130 170	23 126 175
	4	29 76 125 158	29 76 125 158	29 76 125 158	29 76 125 158	29 76 125 158	29 76 127 159	33 80 131 161	21 109 153 175	17 74 131 176
	5	28 71 115 145 172	28 71 115 145 172	28 71 116 146 173	28 71 115 145 172	28 71 115 145 172	28 72 116 146 173	24 50 97 139 172	17 84 130 158 180	17 69 128 165 186
	2	81 140	81 140	81 140	81 140	81 140	81 140	81 141	80 161	93 183
Lena	3	73 119 165	73 119 165	73 119 165	73 119 165	73 119 165	73 119 165	71 118 163	61 122 177	77 148 207
	4	69 107 139 175	69 107 139 175	70 108 140 176	69 107 139 176	70 108 140 176	69 108 140 176	71 110 142 187	58 108 147 189	68 122 171 224
	5	59 86 115 144 178	59 86 115 144 178	59 86 115 143 177	60 87 115 145 180	59 86 115 144 178	60 85 115 144 177	1 61 95 129 173	53 95 127 159 193	65 111 149 182 230
	2	90 145	90 145	90 145	90 145	90 145	90 145	89 144	92 163	120 189
	3	71 110 152	71 110 152	71 110 152	71 110 152	71 110 152	71 110 152	72 109 154	76 131 177	97 151 204
Baboon	4	64 99 131 164	64 99 131 164	64 99 132 165	64 99 131 164	64 99 132 164	64 99 131 163	64 96 129 164	70 119 154 184	86 134 168 211
	5	53 81 109 137 167	53 81 109 137 167	51 80 108 137 167	53 81 108 134 167	53 82 110 138 168	54 81 109 136 168	1 61 101 137 167	62 103 131 157 184	76 117 148 179 214
	2	26 90	26 90	26 90	26 90	26 90	26 90	26 90	28 132	36 172
	3	18 60 116	18 60 116	18 60 116	18 60 116	18 60 116	18 60 116	19 63 119	17 84 147	22 109 191
	4	13 41 83 131	13 41 83 131	13 41 82 130	13 41 83 131	14 43 84 131	13 42 83 131	14 44 85 139	12 60 107 155	16 79 145 202
Pirate	5	10 29 57 94 136	10 29 57 94 136	11 30 58 94 135	10 29 57 94 136	10 30 59 95 137	10 30 58 95 136	8 32 67 107 141	7 35 71 113 157	11 54 105 158 207
	2	97 162	97 162	97 162	97 162	97 162	97 162	96 162	105 203	119 223
	3	78 129 180	78 129 180	78 128 180	78 129 180	78 129 180	78 129 180	79 130 184	99 183 212	105 171 227
	4	63 106 149 192	64 107 150 193	63 106 149 192	63 106 149 192	63 106 149 192	63 106 149 192	62 112 149 188	91 161 198 214	90 139 201 230
	5	61 100 135 175 204	60 100 135 174 203	61 100 135 176 204	60 100 135 174 203	61 100 135 175 204	60 100 134 173 204	62 106 142 185 205	87 149 188 205 216	76 122 171 214 233
Peppers	2	57 130	57 130	57 130	57 130	57 130	57 130	57 130	77 167	89 189
	3	45 88 138	45 88 138	45 88 138	45 88 138	45 88 138	45 88 138	48 88 139	53 117 178	48 115 196
	4	43 83 124 168	43 83 124 168	43 83 125 169	43 83 124 168	43 83 124 168	43 83 124 167	42 85 125 171	41 96 141 185	43 108 166 209
	5	26 53 87 126 169	26 53 87 126 169	25 53 87 125 168	42 80 112 144 176	42 80 112 144 176	23 53 85 126 169	17 54 85 129 168	37 89 125 159 191	33 81 116 171 211
	2	73 134	73 134	73 134	73 134	73 134	73 134	73 134	74 148	88 176
Living room	3	44 94 145	44 94 145	44 94 145	44 94 145	44 94 145	44 94 145	41 92 145	60 124 173	66 144 197
	4	38 83 124 161	38 83 124 161	38 83 125 161	38 83 124 161	38 83 124 161	38 83 124 161	36 76 120 162	47 101 35 175	59 128 170 216
	5	33 69 102 133 167	33 69 102 133 167	33 69 102 134 169	33 69 102 133 167	34 72 105 133 166	34 70 102 133 168	34 66 94 121 158	45 96 126 152 186	51 106 146 181 227
	2	38 122	38 122	38 122	38 122	38 122	38 122	38 122	88 163	110 204
	3	33 107 155	33 107 155	34 107 155	33 107 155	33 107 155	33 107 155	35 108 154	75 134 175	101 172 219
Barbara	4	31 96 132 165	31 96 132 165	31 96 132 165	32 97 134 165	31 96 132 165	31 96 132 165	28 97 130 166	66 117 151 180	98 47 190 226
	5	14 59 99 134 165	14 59 99 134 165	14 58 98 134 166	14 57 98 134 166	14 59 99 134 165	14 60 99 135 164	4 47 101 136 169	67 114 146 166 186	48 105 157 194 227
	2	76 142	76 142	76 142	76 142	76 142	76 142	75 167	92 195	
	3	57 104 161	57 104 161	57 104 162	57 104 161	57 104 161	57 104 161	56 101 163	55 114 188	77 139 222
	4	48 85 125 177	48 85 125 177	45 81 120 174	48 85 125 177	48 85 125 177	48 85 124 178	49 79 121 171	50 96 144 202	63 109 164 235
Bridge	5	43 76 108 146 192	40 72 104 142 190	43 76 108 146 192	43 76 108 146 192	44 76 108 147 193	44 76 108 147 193	32 72 103 143 197	41 80 115 160 206	55 97 138 187 246
	2	89 139	89 139	89 139	89 139	89 139	89 139	89 139	84 156	109 198
	3	77 114 157	77 114 157	77 114 156	77 113 156	77 114 157	77 114 157	76 113 154	70 117 171	95 154 221
	4	70 97 125 161	70 97 125 161	70 97 126 162	70 97 126 162	70 97 125 161	69 103 126 158	67 104 139 180	83 127 173 227	
	5	61 83 105 130 163	61 83 105 130 163	60 82 104 129 162	62 83 103 128 163	61 83 105 130 163	61 82 101 127 162	1 67 92 124 155	57 85 110 140 181	78 114 147 182 230
Butterfly	2	73 141	73 141	73 141	73 141	73 141	73 141	73 141	64 186	71 198
	3	62 105 163	62 105 163	62 105 163	62 105 163	62 106 164	62 105 163	64 109 165	53 118 194	59 124 205
	4	56 90 143 195	56 90 143 195	56 90 143 195	56 90 143 195	56 89 142 194	57 90 144 195	58 86 136 187	48 96 151 202	56 110 188 228
	5	49 73 109 155 197	49 73 109 155 197	49 74 110 156 198	49 73 109 155 197	49 74 110 156 198	49 74 110 155 198	1 61 99 147 192	44 79 121 166 206	52 90 139 192 230

**Table 5**

Comparison of fitness values obtained by HHO, PSO, FFO, DE, HS, ABC and SCA using cross entropy for the set of benchmark images.

Image	nTh	HHO		PSO		FFO		DE		HS		ABC		SCA	
		Mean	Std	Mean	Std	Mean	Std	Mean	Std	Mean	Std	Mean	Std	Mean	Std
Cameraman	2	<b>1.4016</b>	0	<b>1.4016</b>	0	1.4018	0.0002	<b>1.4016</b>	0	<b>1.4016</b>	0	<b>1.4016</b>	0	1.4023	0.0007
	3	<b>0.7638</b>	0	<b>0.7638</b>	0	0.7653	0.0064	<b>0.7638</b>	0	<b>0.7638</b>	3.60E-05	<b>0.7638</b>	1.22E-05	0.7690	0.0031
	4	<b>0.5384</b>	0	<b>0.5384</b>	0	0.5409	0.0113	<b>0.5384</b>	0	<b>0.5384</b>	6.43E-05	0.5386	0.0002	0.5639	0.0377
	5	<b>0.4030</b>	1.53E-05	0.4031	2.14E-05	0.4057	5.05E-03	0.4031	5.95E-05	0.4031	0.0002	0.4039	0.0004	0.4565	0.0418
	Lena	2	<b>1.3662</b>	0	<b>1.3662</b>	0	<b>1.3662</b>	0	<b>1.3662</b>	0	1.3663	2.11E-05	<b>1.3662</b>	0	1.3670
Baboon	2	<b>0.7174</b>	0	<b>0.7174</b>	0	0.7182	0.0019	<b>0.7174</b>	0	<b>0.7174</b>	0	0.7175	3.64E-05	0.7292	0.0072
	3	<b>0.4686</b>	0	0.4687	7.16E-05	0.4697	0.0021	0.4689	0.0004	0.4687	7.52E-05	0.4691	0.0002	0.5057	0.0407
	4	<b>0.3271</b>	0	0.3272	5.14E-05	0.3327	1.19E-02	0.3284	0.0010	0.3290	0.0068	0.3289	0.0012	0.4210	0.0613
	5	<b>1.1905</b>	0	<b>1.1905</b>	0	1.1906	1.80E-05	<b>1.1905</b>	0	<b>1.1905</b>	0	<b>1.1905</b>	0	1.1916	0.0011
	Pirate	2	<b>0.7319</b>	0	0.7320	5.20E-06	0.7320	0.0001	<b>0.7319</b>	0	0.7320	1.09E-05	0.7320	1.09E-05	0.7410
Jetplane	3	<b>0.5001</b>	0	<b>0.5001</b>	0	0.5021	0.0036	0.5002	7.63E-05	0.5001	1.03E-04	0.5005	0.0003	0.5367	0.0518
	4	<b>0.3637</b>	0	0.3638	7.16E-05	0.3660	4.64E-03	0.3647	0.0011	0.3658	3.11E-03	0.3656	0.0012	0.4534	0.0588
	5	<b>2.7409</b>	0	<b>2.7409</b>	0	2.7511	0.0433	<b>2.7409</b>	0	<b>2.7409</b>	0	<b>2.7409</b>	0	2.7411	0.0004
	3	<b>1.6277</b>	0	<b>1.6277</b>	0	1.6546	0.0821	<b>1.6277</b>	0	1.6278	0.0001	1.6278	9.46E-05	1.6338	0.0041
	4	<b>1.0307</b>	2.95E-05	1.0308	4.09E-05	1.1038	0.1487	1.0308	5.61E-05	1.0309	6.50E-05	1.0312	0.0003	1.0600	0.0166
Peppers	5	<b>0.7543</b>	0	<b>0.7543</b>	0	0.8045	0.0664	0.7601	0.0070	0.7757	0.0108	0.7593	0.0038	0.8157	0.0507
	2	<b>0.8209</b>	0	<b>0.8209</b>	0	0.8210	2.95E-05	<b>0.8209</b>	0	<b>0.8209</b>	0	<b>0.8209</b>	0	0.8210	0.0002
	3	<b>0.5086</b>	0	<b>0.5086</b>	0	0.5087	0.0002	0.5087	1.39E-05	0.5087	1.21E-04	0.5087	1.64E-05	0.5125	0.0023
	4	<b>0.3368</b>	0	0.3369	1.10E-05	0.3369	5.13E-05	0.3373	0.0005	0.3369	1.49E-04	0.3370	0.0001	0.3497	0.0065
	5	<b>0.2290</b>	0	0.2291	2.30E-05	0.2300	2.24E-03	0.2301	0.0009	0.2291	1.39E-04	0.2295	0.0003	0.2664	0.0345
Living room	2	<b>1.7332</b>	0	<b>1.7332</b>	0	1.7333	5.15E-05	<b>1.7332</b>	0	<b>1.7332</b>	0	<b>1.7332</b>	0	1.7337	0.0006
	3	<b>1.1608</b>	0	1.1619	0.0037	1.1623	0.0037	1.1624	0.0042	1.1709	0.0054	1.1610	0.0002	1.1697	0.0061
	4	<b>0.7221</b>	0	<b>0.7221</b>	0	0.7228	0.0007	<b>0.7221</b>	0	<b>0.7221</b>	0	<b>0.7221</b>	0	0.7224	0.0003
	5	0.5534	0.0129	0.5549	0.0134	0.5516	0.01609	0.5578	0.0130	0.5702	0.0081	<b>0.5482</b>	0.0028	0.6122	0.0375
	2	<b>1.8735</b>	0	<b>1.8735</b>	0	1.8736	9.52E-05	<b>1.8735</b>	0	<b>1.8735</b>	0	<b>1.8735</b>	0	1.8742	0.0011
Barbara	3	<b>1.1704</b>	0	<b>1.1704</b>	0	1.1706	0.0001	<b>1.1704</b>	0	<b>1.1704</b>	0	1.1705	4.28E-05	1.1759	0.0032
	4	<b>0.7571</b>	0	0.7572	3.56E-06	0.7583	0.0051	<b>0.7571</b>	0	0.7572	3.96E-06	0.7572	0.0001	0.7879	0.0185
	5	<b>0.5391</b>	0	<b>0.5391</b>	0	0.5424	0.0062	0.5392	0.0009	0.5439	0.0024	0.5410	0.0011	0.6286	0.0770
	2	<b>1.5194</b>	0	1.5270	0.0314	1.5215	0.0088	<b>1.5194</b>	0	<b>1.5194</b>	0	<b>1.5194</b>	0	1.5195	0.0002
	3	<b>0.7803</b>	0	<b>0.7803</b>	0	0.7810	0.0027	0.7804	0.0001	<b>0.7803</b>	0	0.7804	7.70E-06	0.7841	0.0031
Bridge	4	0.5302	0.01360	0.5280	1.61E-06	0.5293	0.0038	0.5289	0.0011	<b>0.5279</b>	0	0.5280	0.0001	0.5553	0.0220
	5	<b>0.3767</b>	0	0.3768	0.0001	0.3849	0.01096	0.3855	0.0099	0.3966	0.0171	0.3787	0.0014	0.4162	0.0315
	2	<b>2.4430</b>	0	<b>2.4430</b>	0	2.4431	0.0004	<b>2.4430</b>	0	<b>2.4430</b>	0	<b>2.4430</b>	0	2.4437	0.0010
	3	<b>1.4698</b>	0	<b>1.4698</b>	0	1.4699	0.0002	<b>1.4698</b>	0	1.4699	8.15E-05	1.4699	7.74E-08	1.4775	0.0070
	4	<b>1.0144</b>	1.87E-05	1.01475	0.0007	1.0150	2.31E-03	1.01467	0.0006	1.0162	0.0009	1.0146	0.0003	1.0403	0.0185
Butterfly	5	0.7271	0.0001	0.7274	0.0006	0.7278	0.0022	<b>0.7270</b>	0	0.7277	0.0018	0.7277	0.0008	0.8002	0.0372
	2	<b>1.1830</b>	0	<b>1.1830</b>	0	1.1831	3.60E-05	1.1831	2.14E-05	1.1831	5.55E-05	<b>1.1830</b>	0	1.1833	0.0003
	3	<b>0.6232</b>	0	0.6233	2.75E-05	0.6235	0.0003	0.6233	5.79E-05	0.6233	5.77E-05	0.6233	4.09E-05	0.6355	0.0078
	4	<b>0.4064</b>	0	0.4065	6.85E-05	0.4151	0.0185	0.4079	0.0019	0.4065	6.85E-05	0.4068	0.0003	0.4569	0.0574
	5	<b>0.3037</b>	0	0.3052	0.0048	0.3138	1.57E-02	0.3108	0.0052	0.3141	0.0077	0.3063	0.0012	0.3877	0.0655
Lake	2	<b>1.4382</b>	0	<b>1.4382</b>	0	1.4383	9.87E-05	<b>1.4382</b>	0	<b>1.4382</b>	0	<b>1.4382</b>	0	1.4389	0.0008
	3	<b>0.9624</b>	0	<b>0.9624</b>	0	0.9625	0.0001	<b>0.9624</b>	0	0.9627	0.0003	0.9625	8.73E-05	0.9693	0.0044
	4	<b>0.6313</b>	0	0.6314	2.78E-05	0.6317	0.0009	<b>0.6313</b>	0	0.6314	1.92E-04	0.6315	0.0002	0.6587	0.01690
	5	<b>0.4361</b>	0	0.4362	7.50E-05	0.4366	5.87E-04	0.4363	0.0003	0.4367	0.0005	0.4370	0.0006	0.5176	0.0763

**Table 6**

Comparison of PSNR values obtained by HHO, PSO, FFO, DE, HS, ABC and SCA, K-means and Fuzzy IterAg in the set of benchmark images.

Image	nTh	HHO		PSO		FFO		DE		HS		ABC		SCA		K-means		Fuzzy IterAg	
		Mean	Std	Mean	Std	Mean	Std	Mean	Std	Mean	Std	Mean	Std	Mean	Std	Mean	Std	Mean	Std
Cameraman	2	<b>16.1255</b>	0	<b>16.1255</b>	0	16.1156	0.0237	<b>16.1255</b>	0	<b>16.1255</b>	0	<b>16.1255</b>	0	16.1094	0.0507	12.6221	0.2242	11.6980	0
	3	18.7002	0	18.7002	0	<b>18.7864</b>	1.70E-01	18.7002	0	18.7343	0.0424	18.7002	0	18.6978	0.2446	15.4810	1.9723	16.0535	3.60E-15
	4	<b>21.4058</b>	1.80E-14	<b>21.4058</b>	1.80E-14	21.3458	3.26E-01	<b>21.4058</b>	1.80E-14	21.3992	2.02E-02	<b>21.4058</b>	1.80E-14	20.8372	0.7145	17.5655	3.1587	19.2990	0
	5	22.8623	0.0001	22.8623	0.0001	22.8105	1.47E-01	22.8645	0.0121	<b>22.8684</b>	0.0164	22.8624	7.21E-15	22.1382	0.5988	20.2004	2.1611	20.4128	7.21E-15
	Lena	2	<b>15.7309</b>	9.01E-15	<b>15.7309</b>	9.01E-15	15.7308	9.01E-15	<b>15.7309</b>	9.01E-15	15.729	0.0041	<b>15.7309</b>	9.01E-15	15.7211	0.0137	14.5545	0.0558	14.0230
Baboon	2	<b>17.6160</b>	1.44E-14	<b>17.6160</b>	1.44E-14	17.6152	1.60E-02	<b>17.6160</b>	1.44E-14	<b>17.6160</b>	1.44E-14	<b>17.6160</b>	1.44E-14	17.5742	0.0715	16.8449	1.5789	15.6932	1.80E-15
	3	<b>18.9429</b>	1.44E-14	18.9281	0.0207	18.9177	2.63E-02	18.9345	0.0217	18.9195	0.02174	<b>18.9429</b>	1.44E-14	18.8186	0.2566	18.3366	2.0157	17.6078	1.08E-14
	4	<b>20.3647</b>	1.80E-14	20.3626	0.0079	20.3568	8.29E-02	20.3070	0.0669	20.2984	0.1094	<b>20.3647</b>	1.80E-14	19.9048	0.8089	18.9736	3.6164	18.8577	1.08E-14
	5	18.8189	7.21E-15	18.8199	0.006	<b>18.8421</b>	2.44E-02	18.8189	7.21E-15	18.8240	0.0126	18.8189	7.21E-15	18.8071	0.1392	17.4751	0.9069	15.4697	1.08E-14
	Pirate	2	20.7683	1.08E-14	20.7683	1.08E-14	<b>20.7734</b>	6.97E-02	20.7641	0.0144	20.7419	0.0322	20.7683	1.08E-14	20.4744	0.4501	18.3261	2.9595	17.3539
Jetplane	2	22.7327	1.08E-14	22.7377	0.0126	<b>22.7640</b>	5.07E-02	22.7253	0.0483	22.6929	0.1008	22.7327	1.08E-14	21.5514	0.7784	20.1961	3.0118	19.4333	7.21E-15
	3	16.1520	1.08E-14	16.1520	1.08E-14	<b>16.2137</b>	2.32E-01	16.1520	1.08E-14	16.1520	1.08E-14	16.1520	1.08E-14	16.1337	0.0466	15.1428	0.0513	11.8044	5.41E-15
	4	18.9573	7.21E-15	18.9573	7.21E-15	<b>18.9808</b>	2.79E-01	18.9573	7.21E-15	18.9554	1.10E-02	18.9573	7.21E-15	18.9545	0.1379	17.8265	1.5625	16.5741	1.08E-14
	5	20.9483	0.0207	20.9510	0.0283	21.0038	4.61E-01	20.9579	0.0389	<b>21.0448</b>	0.0446	20.9441	7.21E-15	20.8154	0.3007	19.0614	2.0927	18.4816	1.44E-14
	2	22.2669	0	22.2669	0	22.4993	3.95E-01	22.4463	0.1768	<b>22.8207</b>	0.1538	22.2669	0	21.8497	0.4913	21.1131	1.6966	20.4806	0.0022
Peppers	2	<b>14.9182</b>	7.21E-15	<b>14.9182</b>	7.21E-15	14.8994	2.37E-02	<b>14.9182</b>	7.21E-15	<b>14.9182</b>	7.21E-15	<b>14.9182</b>	7.21E-15	14.9102	0.0658	13.0846	0.1685	9.8526	5.41E-15
	3	18.5816	7.21E-15	18.5816	7.21E-15	<b>18.5969</b>	8.23E-02	18.5856	0.0211	18.5957	5.32E-02	18.5816	7.21E-15	18.4499	0.3591	15.4691	2.9068	15.3914	3.60E-15
	4	21.2084	1.44E-14	21.2272	0.0196	21.2237	2.28E-02	21.2035	0.0776	<b>21.2364</b>	0.0382	21.2084	1.44E-14	20.8381	0.4010	16.8050	4.0018	17.4377	3.60E-15
	5	22.8346	1.08E-14	22.8573	0.0337	22.8207	9.04E-02	22.8035	0.1432	<b>22.8597</b>	0.0480	22.8346	1.08E-14	22.1965	0.8328	19.3910	3.0817	18.8345	1.44E-14
	2	15.4951	0	15.4951	0	15.5014	0.0219	15.4951	0	15.4951	0	15.4951	0	<b>15.5388</b>	0.0631	15.0894	0.2478	13.4779	9.01E-15
Living room	3	17.8358	7.21E-15	17.8442	0.0279	17.8589	4.88E-02	17.8566	0.0484	<b>17.9027</b>	0.0433	17.8358	7.21E-15	17.8479	0.2055	17.0590	0.5700	15.0772	3.60E-15
	4	20.4377	3.60E-15	20.4377	3.60E-15	<b>20.4480</b>	3.94E-02	20.4377	3.60E-15	20.4377	3.60E-15	20.4377	3.60E-15	20.2081	0.3057	18.5421	1.8794	17.0241	7.21E-15
	5	21.5783	0.3173	21.6168	0.3303	21.4153	2.03E-01	21.6188	0.3456	<b>21.9504</b>	0.2316	21.4242	0.1913	20.9568	0.5464	20.1771	2.0874	19.7108	7.21E-15
	2	<b>16.3059</b>	7.21E-15	<b>16.3059</b>	7.21E-15	16.3033	2.52E-02	<b>16.3059</b>	7.21E-15	<b>16.3059</b>	7.21E-15	<b>16.3059</b>	7.21E-15	16.2826	0.0780	15.1398	0.2962	14.2855	1.08E-14
	3	18.3916	1.08E-14	18.3916	1.08E-14	18.4227	3.94E-02	18.3916	1.08E-14	18.3916	1.08E-14	18.3916	1.08E-14	<b>18.4359</b>	0.2105	17.2447	0.6205	15.1946	5.41E-15
Barbara	2	20.4402	1.44E-14	20.4314	0.0198	20.3690	4.96E-02	<b>20.4402</b>	1.44E-14	20.4284	0.0220	<b>20.4402</b>	1.44E-14	20.1835	0.2801	19.8417	0.7997	17.1314	7.21E-15
	3	<b>22.2828</b>	7.21E-15	<b>22.2828</b>	7.21E-15	22.1753	1.13E-01	22.2826	0.0053	22.2580	0.0344	<b>22.2828</b>	7.21E-15	21.2750	0.6125	20.7487	1.9702	19.9100	0.0029
	4	14.7982	7.21E-15	14.8051	0.0280	<b>14.8069</b>	2.12E-01	14.7982	7.21E-15	14.7982	7.21E-15	14.7982	7.21E-15	14.7972	0.0636	14.4996	0.3406	12.1482	0.8555
	5	17.4780	3.60E-15	17.4780	3.60E-15	<b>17.5635</b>	1.92E-01	17.4849	0.0318	17.4780	3.60E-15	17.4780	3.60E-15	17.5041	0.2611	17.5929	1.1542	13.8449	9.01E-15
	2	19.2190	0.1209	19.2017	0.0185	<b>19.3181</b>	1.37E-01	19.2329	0.1450	19.1986	3.60E-15	19.1986	3.60E-15	18.7825	0.7323	19.1951	2.4357	15.3499	5.41E-15
Bridge	3	22.1681	7.21E-15	22.1599	0.0197	<b>22.2099</b>	4.83E-01	22.0124	0.3885	21.5212	0.9014	22.1681	7.21E-15	21.1295	0.7586	20.1545	3.3177	18.6724	0.0269
	2	<b>14.9625</b>	9.01E-15	<b>14.9625</b>	9.01E-15	14.9546	2.84E-02	<b>14.9625</b>	9.01E-15	<b>14.9625</b>	9.01E-15	<b>14.9625</b>	9.01E-15	14.9106	0.0641	14.4433	0.2743	13.2014	7.21E-15
	3	<b>17.6314</b>	0	<b>17.6314</b>	0	17.6215	0.0461	<b>17.6314</b>	0	17.6273	0.0137	<b>17.6314</b>	0	17.4745	0.1013	16.4107	1.4185	15.8283	3.60E-15
	4	19.5325	0.0156	19.5279	0.0194	19.4625	0.0792	<b>19.5411</b>	0.0055	19.5316	0.01940	19.5360	0.0116	19.1908	0.1383	17.8290	2.4937	17.9631	3.60E-15
	5	21.1322	0.0265	21.1350	0.0282	21.1290	7.63E-02	<b>21.1443</b>	0.0285	21.1194	0.0550	21.1387	0.0280	20.2892	0.4779	17.8307	4.3320	19.4389	3.60E-15
Butterfly	2	14.9160	9.01E-15	14.9160	9.01E-15	14.9270	3.66E-02	14.9196	0.0217	<b>14.9415</b>	0.0523	14.9160	9.01E-15	14.9250	0.1106	14.9783	0.3355	11.8810	0
	3	17.4597	1.44E-14	17.4590	4.30E-03	<b>17.4881</b>	6.97E-02	17.4579	0.0062	17.4561	0.0090	17.4597	1.44E-14	17.4487	0.3780	17.6472	0.7785	14.1798	1.08E-14
	4	19.3029	1.44E-14	19.3206	0.03962	<b>19.4494</b>	2.33E-01	19.3482	0.0918	19.3206	0.0396	19.3029	1.44E-14	19.1632	0.6633	18.9256	2.1744	16.6159	3.60E-15
	5	<b>21.5344</b>	7.21E-15	21.3765	0.4209	21.3954	6.47E-01	21.2758	0.5155	20.5639	0.6282	<b>21.5344</b>	7.21E-15	20.3617	1.2486	21.2026	1.2090	17.8806	3.60E-15
	2	<b>14.3009</b>	9.01E-15	<b>14.3009</b>	9.01E-15	14.2895	2.55E-02	<b>14.3009</b>	9.01E-15	<b>14.3009</b>	9.01E-15	<b>14.3009</b>	9.01E-15	14.2852	0.0673	12.4182	0.2557	11.3697	5.41E-15
Lake	3	16.7352	0	16.7352	0	16.7399	0.0161	16.7352	0	<b>16.7519</b>	0.0472	16.7352	0	16.6965	0.1716	15.3194	0.7138	15.3558	1.08E-14
	4	<b>17.9987</b>	0	17.9950	0.0105	17.9552	0.0700	<b>17.9987</b>	0	17.9550	0.0395	<b>17.9987</b>	0	17.8420	0.4168	16.8333	2.6243	15.6761	1.08E-14
	5	20.0846	7.21E-15	<b>20.0888</b>	0.0195	20.0810	7.97E-02	20.0798	0.0516	20.0682	0.0662	20.0846	7.21E-15	19.4053	0.9318	18.0712	3.3553	18.2789	7.21E-15

**Table 7**

Comparison of SSIM values obtained by HHO, PSO, FFO, DE, HS, ABC and SCA, K-means and Fuzzy IterAg in the set of benchmark images.

Image	nTh	HHO		PSO		FFO		DE		HS		ABC		SCA		K-Means		Fuzzy IterAg		
		Mean	Std	Mean	Std	Mean	Std	Mean	Std											
Cameraman	2	<b>0.6167</b>	1.13E-16	<b>0.6167</b>	1.13E-16	0.6165	7.51E-04	<b>0.6167</b>	1.13E-16	<b>0.6167</b>	1.13E-16	<b>0.6167</b>	1.13E-16	0.6163	0.0015	0.4696	0.0080	0.4115	0	
	3	0.6694	4.51E-16	0.6694	4.51E-16	0.6688	3.11E-03	0.6694	4.51E-16	<b>0.6700</b>	0.0006	0.6694	4.51E-16	0.6682	0.0109	0.5469	0.0875	0.5776	1.13E-16	
	4	<b>0.6955</b>	3.38E-16	<b>0.6955</b>	3.38E-16	0.6921	7.19E-03	<b>0.6955</b>	3.38E-16	0.6949	1.39E-03	<b>0.6955</b>	3.38E-16	0.6790	0.0181	0.5975	0.1037	0.6706	1.13E-16	
	5	0.7185	8.02E-05	0.7185	0.0001	0.7167	0.00569	0.7185	0.0002	0.7182	0.0007	<b>0.7186</b>	0	0.7074	0.0139	0.6821	0.0768	0.6466	5.63E-16	
	Lena	2	<b>0.5765</b>	1.13E-16	<b>0.5765</b>	1.13E-16	<b>0.5765</b>	1.13E-16	<b>0.5765</b>	1.13E-16	0.5761	0.0011	<b>0.5765</b>	1.13E-16	0.5748	0.0027	0.5370	0.0066	0.5174	1.13E-16
Baboon	3	<b>0.6499</b>	0	<b>0.6499</b>	0	0.6493	0.0021	<b>0.6499</b>	0	<b>0.6499</b>	0	<b>0.6499</b>	0	0.6465	0.0064	0.6240	0.0731	0.5518	3.38E-16	
	4	<b>0.6845</b>	3.38E-16	0.6836	0.0011	0.6830	1.41E-03	0.6840	0.0011	0.6831	0.0012	<b>0.6845</b>	3.38E-16	0.6828	0.0097	0.6607	0.0655	0.6422	4.51E-16	
	5	<b>0.7362</b>	4.51E-16	0.7361	0.0002	0.7340	5.72E-03	0.7346	0.0020	0.7337	0.0058	<b>0.7362</b>	4.51E-16	0.7183	0.0270	0.6859	0.0870	0.6814	2.25E-16	
	Pirate	2	<b>0.6352</b>	5.63E-16	<b>0.6352</b>	5.63E-16	0.6351	5.81E-05	0.6352	5.63E-16	<b>0.6352</b>	5.63E-16	<b>0.6352</b>	5.63E-16	0.6350	0.0023	0.5878	0.0268	0.4148	1.69E-16
	3	0.7387	0	0.7387	0.0002	0.7397	9.89E-04	0.7387	0	<b>0.7389</b>	0.0005	0.7387	0	0.7379	0.0052	0.6807	0.0241	0.6182	2.25E-16	
Jetplane	4	<b>0.8045</b>	0	<b>0.8045</b>	0	0.8044	0.0015	0.8044	0.0003	0.8042	0.0004	<b>0.8045</b>	0	0.7925	0.0153	0.7042	0.1470	0.6996	3.38E-16	
	5	0.8486	4.51E-16	0.8487	0.0002	<b>0.8489</b>	9.94E-04	0.8484	0.0009	0.8471	0.0025	0.8486	4.51E-16	0.8213	0.0182	0.7691	0.1305	0.7588	2.25E-16	
	Peppers	2	<b>0.5246</b>	2.25E-16	<b>0.5246</b>	2.25E-16	0.5236	3.61E-03	<b>0.5246</b>	2.25E-16	<b>0.5246</b>	2.25E-16	<b>0.5246</b>	2.25E-16	0.5243	0.0004	0.4284	0.0049	0.3311	0
	3	<b>0.6108</b>	4.51E-16	<b>0.6108</b>	4.51E-16	0.6063	1.26E-02	<b>0.6108</b>	4.51E-16	0.6107	1.66E-04	<b>0.6108</b>	4.51E-16	0.6095	0.0017	0.5308	0.0615	0.4932	5.63E-17	
	4	0.6804	6.01E-05	0.6804	2.82E-05	0.6698	0.0188	0.6804	3.87E-05	<b>0.6805</b>	8.46E-05	0.6804	0	0.6774	0.0053	0.5988	0.0762	0.5598	0	
Living room	5	<b>0.7328</b>	3.38E-16	<b>0.7328</b>	3.38E-16	0.7186	1.49E-02	0.7294	0.0029	0.7238	0.0032	<b>0.7328</b>	3.38E-16	0.7300	0.0115	0.6890	0.0516	0.6261	5.81E-05	
	Barbara	2	<b>0.7422</b>	3.38E-16	<b>0.7422</b>	3.38E-16	0.7416	7.07E-04	0.7422	3.38E-16	<b>0.7422</b>	3.38E-16	<b>0.7422</b>	3.38E-16	0.7420	0.0009	0.5139	0.0054	0.5641	3.38E-16
	3	<b>0.8040</b>	3.38E-16	<b>0.8040</b>	3.38E-16	0.8036	6.86E-04	0.8039	0.0003	0.8037	8.61E-04	<b>0.8040</b>	3.38E-16	0.8031	0.0051	0.5890	0.1253	0.7372	3.38E-16	
	4	<b>0.8050</b>	0	0.8024	0.0027	0.8037	0.0024	0.8014	0.0075	0.8010	0.0045	<b>0.8050</b>	0	0.8013	0.0261	0.6345	0.1338	0.6517	3.38E-16	
	5	0.7960	1.13E-16	0.7968	0.0011	0.7970	4.98E-03	<b>0.7961</b>	0.0042	0.7969	0.0015	0.7960	1.13E-16	0.7943	0.0224	0.7215	0.0811	0.7494	0	
Bridge	2	<b>0.6479</b>	0	<b>0.6479</b>	0	0.6478	8.71E-05	<b>0.6479</b>	0	<b>0.6479</b>	0	<b>0.6479</b>	0	0.6478	0.0004	0.5571	0.0156	0.4846	2.82E-16	
	3	<b>0.6957</b>	1.13E-16	0.6928	0.0096	0.6925	9.64E-03	0.6915	0.0109	0.6703	0.0153	<b>0.6957</b>	1.13E-16	0.6902	0.0100	0.6172	0.0172	0.6170	3.38E-16	
	4	0.7154	2.25E-16	0.7154	2.25E-16	<b>0.7156</b>	6.70E-04	0.7154	2.25E-16	0.7154	2.25E-16	0.7154	2.25E-16	0.7146	0.0053	0.6544	0.0578	0.6222	1.13E-16	
	5	0.7540	0.0067	0.7532	0.0069	0.7561	7.96E-03	0.7520	0.0067	0.7447	0.0048	<b>0.7573</b>	0.0040	0.7490	0.0113	0.6890	0.0454	0.7088	3.38E-16	
	Barbara	2	0.5453	2.25E-16	0.5453	2.25E-16	<b>0.5454</b>	1.13E-03	0.5453	2.25E-16	0.5453	2.25E-16	0.5453	2.25E-16	0.5453	0.0027	0.5131	0.0088	0.4820	2.82E-16
Butterfly	3	0.6580	4.51E-16	0.6580	4.51E-16	<b>0.6585</b>	4.14E-04	0.6580	4.51E-16	0.6580	4.51E-16	0.6580	4.51E-16	0.6571	0.0034	0.5890	0.0308	0.5207	1.13E-16	
	4	<b>0.7147</b>	2.25E-16	<b>0.7147</b>	5.10E-05	0.7132	2.36E-03	<b>0.7147</b>	2.25E-16	<b>0.7147</b>	5.68E-05	<b>0.7147</b>	2.25E-16	<b>0.7147</b>	0.0089	0.6818	0.0309	0.5817	0	
	5	<b>0.7628</b>	5.63E-16	<b>0.7628</b>	5.63E-16	0.7591	3.25E-03	0.7627	0.0006	0.7596	0.0015	<b>0.7628</b>	5.63E-16	0.7418	0.0167	0.7140	0.0560	0.6781	7.95E-05	
	Barbara	2	0.5906	3.38E-16	0.5862	0.0181	<b>0.5915</b>	1.08E-02	0.5906	3.38E-16	0.5906	3.38E-16	0.5906	3.38E-16	0.5901	0.0035	0.4850	0.0150	0.4268	0.0529
	3	0.6418	2.25E-16	0.6418	2.25E-16	<b>0.6455</b>	6.97E-03	0.6421	0.0012	0.6418	2.25E-16	0.6418	2.25E-16	0.6446	0.0103	0.5897	0.0484	0.4506	3.38E-16	
Lake	4	0.7049	0.0015	0.7047	0.0005	<b>0.7079</b>	5.80E-03	0.7069	0.0047	0.7046	5.63E-16	0.7046	5.63E-16	0.6885	0.0243	0.6501	0.0820	0.5052	0	
	5	<b>0.7704</b>	4.51E-16	0.7701	0.0008	0.7677	9.70E-03	0.7641	0.0103	0.7540	0.0151	<b>0.7704</b>	4.51E-16	0.7499	0.0170	0.6904	0.1034	0.6595	0.0013	
	Pirate	2	<b>0.5066</b>	2.25E-16	<b>0.5066</b>	2.25E-16	0.5063	7.51E-04	<b>0.5066</b>	2.25E-16	<b>0.5066</b>	2.25E-16	<b>0.5066</b>	2.25E-16	0.5053	0.0027	0.4639	0.0223	0.3880	1.69E-16
	3	0.6560	4.51E-16	0.6560	4.51E-16	<b>0.6567</b>	2.11E-03	0.6560	4.51E-16	0.6564	0.0011	0.6560	4.51E-16	0.6504	0.0062	0.5915	0.0771	0.5315	1.13E-16	
	4	0.7364	0.0018	0.7367	0.0023	<b>0.7373</b>	0.0032	0.7353	0.0008	0.7344	0.0012	0.7360	0.0013	0.7288	0.0073	0.6677	0.0888	0.6447	2.25E-16	
Butterfly	5	0.7904	0.0011	<b>0.7923</b>	0.0012	0.7901	1.44E-03	0.7903	0.0006	0.7909	0.0017	0.7903	0.0009	0.7721	0.0165	0.6995	0.1163	0.7153	4.51E-16	
	2	0.4619	1.13E-16	0.4619	1.13E-16	0.4624	1.80E-03	0.4621	0.0010	<b>0.4631</b>	0.0026	0.4619	1.13E-16	0.4621	0.0053	0.4752	0.0212	0.3088	1.13E-16	
	3	0.5890	2.25E-16	0.5890	4.74E-06	<b>0.5905</b>	2.62E-03	0.5890	2.59E-05	0.5890	9.95E-06	0.5890	2.25E-16	0.5865	0.0150	0.5835	0.0414	0.4347	0	
	4	0.6629	2.25E-16	0.6635	0.0013	0.6631	6.70E-03	<b>0.6639</b>	0.0033	0.6635	0.0013	0.6629	2.25E-16	0.6563	0.0235	0.6318	0.0721	0.5358	2.25E-16	
	5	<b>0.7360</b>	3.38E-16	0.7322	0.0119	0.7290	1.88E-02	0.7275	0.0147	0.7074	0.0191	<b>0.7360</b>	3.38E-16	0.6964	0.0367	0.7141	0.0412	0.6015	3.38E-16	
Lake	2	<b>0.5279</b>	0	<b>0.5279</b>	0	0.5278	3.82E-05	<b>0.5279</b>	0	<b>0.5279</b>	0	<b>0.5279</b>	0	0.5271	0.0013	0.3643	0.0031	0.3721	2.82E-16	
	3	<b>0.5994</b>	3.38E-16	<b>0.5994</b>	3.38E-16	0.5990	1.50E-03	<b>0.5994</b>	3.38E-16	0.5972	0.0026	<b>0.5994</b>	3.38E-16	0.5970	0.0113	0.5360	0.0324	0.5587	3.38E-16	
	4	<b>0.6309</b>	0	0.6308	0.0002	0.6288	0.0034	<b>0.6309</b>	0	0.6293	0.0025	<b>0.6309</b>	0	0.6242	0.0195	0.5943	0.0878	0.5313	0	
	5	<b>0.7038</b>	3.38E-16	0.7037	0.0001	0.7031	3.25E-03	0.7036	0.0011	0.7015	0.0048	<b>0.7038</b>	3.38E-16	0.6871	0.0444	0.6515	0.0995	0.6477	3.38E-16	

**Table 8**

Comparison of FSIM values obtained by the HHO, PSO, FFO, DE, HS, ABC, SCA, K-means and Fuzzy IterAg in the set of benchmark images.

Image	nTh	HHO		PSO		FFO		DE		HS		ABC		SCA		K-means		Fuzzy IterAg		
		Mean	Std	Mean	Std	Mean	Std	Mean	Std											
Cameraman	2	<b>0.7568</b>	0	<b>0.7568</b>	0	0.7567	0.0004	<b>0.7568</b>	0	<b>0.7568</b>	0	<b>0.7568</b>	0	0.7567	0.0010	0.6828	0.0061	0.6656	3.38E-16	
	3	0.8201	5.63E-16	0.8201	5.63E-16	0.8199	2.38E-03	0.8201	5.63E-16	<b>0.8208</b>	0.0008	0.8201	5.63E-16	0.8178	0.0082	0.7266	0.0241	0.7429	3.38E-16	
	4	<b>0.8546</b>	7.89E-16	<b>0.8546</b>	7.89E-16	0.8533	5.28E-03	<b>0.8546</b>	7.89E-16	0.8544	5.02E-04	<b>0.8546</b>	7.89E-16	0.8425	0.0139	0.7696	0.0552	0.8246	6.76E-16	
	5	0.8824	8.49E-05	0.8824	0.0001	0.8817	0.0029	0.8823	0.0001	0.8822	0.0005	0.8824	0	<b>0.8670</b>	0.0123	0.8185	0.0415	0.8233	3.38E-16	
	Lena	2	<b>0.7118</b>	0	<b>0.7118</b>	0	<b>0.7118</b>	0	<b>0.7118</b>	0	0.7117	0.0004	<b>0.7118</b>	0	0.7112	0.0011	0.6810	0.0095	0.6594	4.51E-16
Baboon	2	<b>0.7662</b>	7.89E-16	<b>0.7662</b>	7.89E-16	0.7652	1.53E-03	<b>0.7662</b>	7.89E-16	<b>0.7662</b>	7.89E-16	<b>0.7662</b>	7.89E-16	0.7650	0.0046	0.7398	0.0169	0.7076	2.25E-16	
	3	<b>0.8019</b>	1.13E-16	0.8016	0.0004	0.8016	1.34E-03	0.8017	0.0005	0.8014	0.0005	<b>0.8019</b>	1.13E-16	0.7979	0.0092	0.7751	0.0259	0.7577	3.38E-16	
	4	0.8299	2.25E-16	0.8298	0.0004	<b>0.8301</b>	2.73E-03	0.8296	0.0016	0.8304	0.0010	0.8299	2.25E-16	0.8135	0.0124	0.7992	0.0355	0.8072	4.51E-16	
	5	<b>0.8554</b>	4.51E-16	<b>0.8554</b>	4.51E-16	0.8553	3.11E-04	<b>0.8554</b>	4.51E-16	<b>0.8554</b>	4.51E-16	<b>0.8554</b>	4.51E-16	0.8548	0.0020	0.8453	0.0125	0.7405	3.38E-16	
	Pepper	2	0.8959	5.63E-16	0.8960	9.94E-05	<b>0.8963</b>	6.29E-04	0.8959	5.63E-16	0.8960	0.0002	0.8959	5.63E-16	0.8958	0.0040	0.8945	0.0095	0.8546	1.13E-16
Pirate	3	0.9284	5.63E-16	0.9284	5.63E-16	<b>0.9298</b>	2.65E-03	0.9283	0.0003	0.9280	0.0006	0.9284	5.63E-16	0.9225	0.0094	0.9072	0.0492	0.8961	7.89E-16	
	4	0.9466	4.51E-16	0.9468	0.0004	<b>0.9490</b>	2.41E-03	0.9467	0.0017	0.9472	0.0010	0.9466	4.51E-16	0.9342	0.0113	0.9268	0.0473	0.9221	1.13E-16	
	5	0.7691	5.63E-16	0.7691	5.63E-16	<b>0.7693</b>	2.46E-03	0.7691	5.63E-16	0.7691	5.63E-16	0.7691	5.63E-16	0.7683	0.0010	0.7112	0.0048	0.6453	2.25E-16	
	Jetplane	2	0.8440	5.63E-16	0.8440	5.63E-16	<b>0.8453</b>	5.13E-03	0.8440	5.63E-16	0.8439	4.11E-04	0.8440	5.63E-16	0.8429	0.0038	0.8120	0.0372	0.7616	3.38E-16
	5	0.9188	3.38E-16	0.9188	3.38E-16	0.9243	5.31E-03	0.9220	0.0028	<b>0.9278</b>	0.0021	0.9188	3.38E-16	0.9105	0.0087	0.9001	0.0253	0.8870	7.46E-05	
Peppers	2	<b>0.8055</b>	4.51E-16	<b>0.8055</b>	4.51E-16	0.8052	3.88E-04	<b>0.8055</b>	4.51E-16	<b>0.8055</b>	4.51E-16	<b>0.8055</b>	4.51E-16	0.8054	0.0011	0.6808	0.0022	0.6915	4.51E-16	
	3	0.8677	1.13E-16	0.8677	1.13E-16	0.8670	9.60E-04	0.8676	0.0002	<b>0.8678</b>	3.31E-04	0.8677	1.13E-16	0.8649	0.0027	0.7506	0.0498	0.8133	4.51E-16	
	4	<b>0.8895</b>	5.63E-16	0.8885	0.0010	0.8891	8.31E-04	0.8881	0.0021	0.8883	0.0011	<b>0.8895</b>	5.63E-16	0.8867	0.0086	0.7885	0.0822	0.7970	3.38E-16	
	5	0.9137	3.38E-16	0.9143	0.0008	0.9140	1.98E-03	0.9133	0.0029	<b>0.9147</b>	0.0011	0.9137	3.38E-16	0.9021	0.0154	0.8495	0.0632	0.8462	4.51E-16	
	Living room	2	<b>0.7359</b>	1.13E-16	<b>0.7359</b>	1.13E-16	<b>0.7359</b>	1.18E-04	<b>0.7359</b>	1.13E-16	<b>0.7359</b>	1.13E-16	<b>0.7359</b>	1.13E-16	0.7356	0.0003	0.6911	0.0050	0.6466	3.38E-16
Barbara	3	0.7718	4.51E-16	0.7730	0.0038	0.7727	0.0040	0.7734	0.0044	<b>0.7820</b>	0.0062	0.7718	4.51E-16	0.7713	0.0044	0.7523	0.0128	0.7443	1.13E-16	
	4	0.8215	3.38E-16	0.8215	3.38E-16	<b>0.8222</b>	4.84E-04	0.8215	3.38E-16	0.8215	3.38E-16	0.8215	3.38E-16	0.8187	0.0029	0.7873	0.0237	0.7774	4.51E-16	
	5	0.8420	0.0114	0.8434	0.0119	0.8367	0.0068	0.8435	0.0118	<b>0.8556</b>	0.0080	0.8365	0.0069	0.8280	0.0067	0.8223	0.0226	0.8139	5.63E-16	
	Bridge	2	<b>0.7580</b>	3.38E-16	<b>0.7580</b>	3.38E-16	0.7578	4.07E-04	<b>0.7580</b>	3.38E-16	<b>0.7580</b>	3.38E-16	<b>0.7580</b>	3.38E-16	0.7577	0.0006	0.7421	0.0085	0.7138	5.63E-16
	3	0.8245	6.76E-16	0.8245	6.76E-16	<b>0.8252</b>	7.09E-04	0.8245	6.76E-16	0.8245	6.76E-16	0.8245	6.76E-16	0.8239	0.0029	0.8080	0.0146	0.7618	4.51E-16	
Butterfly	4	<b>0.8820</b>	5.63E-16	0.8819	0.0001	0.8815	6.56E-04	<b>0.8820</b>	5.63E-16	0.8819	0.0001	<b>0.8820</b>	5.63E-16	0.8760	0.0051	0.8673	0.0131	0.8111	5.63E-16	
	5	0.9109	0	0.9109	0	<b>0.9113</b>	0.0010	0.9110	0.0002	0.9122	0.0005	0.9109	0	0.8947	0.0107	0.8880	0.0270	0.8707	0.0001	
	Barbara	2	0.7144	0	<b>0.7167</b>	0.0097	0.7148	0.0049	0.7144	0	0.7144	0	0.7144	0	0.7145	0.0016	0.7204	0.0052	0.6510	0.0243
	4	0.8733	0.0057	0.8743	0.0002	0.8742	1.97E-03	0.8735	0.0020	<b>0.8743</b>	3.38E-16	<b>0.8743</b>	3.38E-16	0.8606	0.0119	0.8446	0.0426	0.7641	2.25E-16	
	5	0.9001	4.51E-16	0.9000	0.0002	0.9013	3.33E-03	0.8991	0.0044	<b>0.9034</b>	0.0041	0.9001	4.51E-16	0.8857	0.0089	0.8742	0.0589	0.8191	0.0009	
Lake	2	<b>0.7748</b>	4.51E-16	<b>0.7748</b>	4.51E-16	0.7746	4.61E-04	<b>0.7748</b>	4.51E-16	<b>0.7748</b>	4.51E-16	<b>0.7748</b>	4.51E-16	0.7742	0.0007	0.7603	0.0055	0.7377	3.38E-16	
	3	<b>0.8469</b>	3.38E-16	<b>0.8469</b>	3.38E-16	0.8463	2.39E-03	0.8469	3.38E-16	0.8465	0.0011	<b>0.8469</b>	3.38E-16	0.8454	0.0032	0.8286	0.0252	0.8154	2.25E-16	
	4	0.8852	0.0007	0.8855	0.0018	0.8847	0.0018	0.8859	0.0010	<b>0.8888</b>	0.0019	0.8854	0.0005	0.8831	0.0065	0.8736	0.0328	0.8628	4.51E-16	
	5	0.9168	0.0004	0.9159	0.0015	0.9168	0.0014	<b>0.9169</b>	0.0001	0.9161	0.0020	0.9168	0.0002	0.9033	0.0100	0.8820	0.0486	0.8965	4.51E-16	
	Butterfly	2	0.7439	3.38E-16	0.7439	3.38E-16	<b>0.7440</b>	2.04E-04	0.7439	0.0001	0.7439	3.38E-16	0.7434	0.0013	0.7281	0.0064	0.6685	2.25E-16		
Lake	3	0.8084	3.38E-16	0.8084	7.02E-05	<b>0.8086</b>	7.84E-04	0.8084	0.0001	0.8084	0.0001	0.8084	3.38E-16	0.8064	0.0050	0.7929	0.0095	0.7283	3.38E-16	
	4	0.8494	1.13E-16	0.8496	0.0004	<b>0.8509</b>	1.81E-03	0.8500	0.0012	0.8496	0.0004	0.8494	1.13E-16	0.8423	0.0124	0.8360	0.0306	0.7924	6.76E-16	
	5	<b>0.8867</b>	6.76E-16	0.8854	0.0024	0.8863	5.45E-03	0.8841	0.0043	0.8815	0.0038	<b>0.8867</b>	6.76E-16	0.8636	0.0205	0.8744	0.0157	0.8400	3.38E-16	
	Barbara	2	<b>0.8354</b>	5.63E-16	<b>0.8354</b>	5.63E-16	0.8353	3.22E-04	<b>0.8354</b>	5.63E-16	<b>0.8354</b>	5.63E-16	<b>0.8354</b>	5.63E-16	0.8349	0.0009	0.7127	0.0025	0.7201	4.51E-16
	3	0.8703	1.13E-16	0.8703	1.13E-16	0.8704	2.05E-04	0.8703	1.13E-16	<b>0.8706</b>	0.0006	0.8703	1.13E-16	0.8690	0.0021	0.8063	0.0294	0.8458	4.51E-16	
Lake	4	<b>0.8833</b>	4.51E-16	0.8832	0.0002	0.8831	9.03E-04	<b>0.8833</b>	4.51E-16	0.8830	0.0005	<b>0.8833</b>	4.51E-16	0.8821	0.0065	0.8486	0.0437	0.8330	4.51E-16	
	5	0.9003	4.51E-16	0.9005	0.0005	<b>0.9012</b>	1.21E-03	0.9005	0.0007	0.9008	0.0010	0.9003	4.51E-16	0.8975	0.0115	0.8779	0.0416	0.8833	2.25E-16	

**Table 9**

Comparison of computational time values obtained with HHO, PSO, FFO, DE, HS, ABC and SCA, K-means and Fuzzy IterAg in the set of benchmark images.

Image	nTh	HHO		PSO		FFO		DE		HS		ABC		SCA		K Means		Fuzzy IterAg		
		Mean	Std	Mean	Std	Mean	Std	Mean	Std	Mean	Std	Mean	Std	Mean	Std	Mean	Std	Mean	Std	
Cameraman	2	0.5138	0.2856	0.6296	0.6416	0.7881	0.4505	0.5256	0.2838	<b>0.4585</b>	0.2626	1.7015	0.5796	0.5208	0.2405	7.3757	0.4903	0.6150	0.3339	
	3	<b>0.4213</b>	0.0352	0.4839	0.0978	0.6388	0.1839	0.5119	0.1127	0.5267	0.0922	1.7950	0.3290	0.4343	0.1078	7.4465	0.4182	0.6470	0.0941	
	4	0.3943	0.0411	0.8932	0.2519	0.6153	0.1493	0.4775	0.0462	0.4285	0.0244	1.3487	0.0853	<b>0.3611</b>	0.0352	7.5053	0.2650	1.8596	0.7080	
	5	0.3956	0.0428	0.8368	0.0970	0.6076	0.1698	0.4984	0.1253	0.4479	0.0338	1.3549	0.0725	<b>0.3777</b>	0.0461	7.8492	0.2447	2.9596	0.4868	
	Lena	2	0.5898	0.0307	0.7946	0.2732	1.2060	0.2131	0.6749	0.0819	0.3723	0.0110	1.5753	0.2188	<b>0.3310</b>	0.1072	6.9817	0.2933	0.4533	0.0232
Baboon	3	0.8228	0.0104	0.8187	0.1169	1.4189	0.3296	0.7650	0.1797	<b>0.3914</b>	0.0092	1.4671	0.2100	0.4245	0.3703	7.0906	0.2590	1.6309	0.2924	
	4	0.6596	0.0136	0.7910	0.1645	2.2210	0.6876	0.7319	0.1120	<b>0.4134</b>	0.0109	1.5103	0.1685	0.5317	0.1397	7.2704	0.2024	2.0780	0.2479	
	5	0.5973	0.0101	0.7963	0.0868	2.5735	0.7206	0.7585	0.0862	<b>0.4318</b>	0.0122	1.5336	0.1385	0.6608	0.3870	7.6031	0.3025	2.2917	0.3474	
	Pirate	2	0.5093	0.0097	0.7315	0.1356	1.9509	0.4922	0.6697	0.0592	<b>0.3739</b>	0.0201	1.4734	0.2478	0.5508	0.2273	27.2840	0.8020	2.4382	0.1199
	3	0.4781	0.0083	0.7092	0.0891	1.8480	0.4386	0.7288	0.0965	<b>0.3867</b>	0.0143	1.4495	0.1889	0.4453	0.1214	43.7168	17.8267	4.9633	0.7442	
Jetplane	4	0.4238	0.0083	0.9000	0.2779	1.9102	0.3983	0.8845	0.2586	0.5043	0.4072	1.5679	0.1306	<b>0.3949</b>	0.0840	55.1584	42.1987	15.0821	1.9213	
	5	<b>0.3798</b>	0.0172	0.9344	0.2061	2.7490	0.8350	0.7013	0.0918	0.4491	0.0303	1.5122	0.1260	0.4597	0.1296	28.8495	2.3431	15.8128	2.4095	
	Pirate	2	0.3746	0.0630	0.7783	0.1768	1.9057	0.4404	0.6284	0.0371	0.3896	0.0481	1.1658	0.2335	<b>0.2890</b>	0.0217	26.6531	1.4249	1.7787	0.1226
	3	0.3939	0.0318	0.7893	0.2011	1.9600	0.4294	0.6626	0.0610	0.4047	0.0266	1.0604	0.1188	<b>0.3116</b>	0.0299	27.0238	0.9592	6.5426	0.6303	
	4	0.4168	0.0322	0.7669	0.1048	2.2633	0.5670	0.6716	0.0340	0.4225	0.0099	1.1920	0.2164	<b>0.3266</b>	0.0245	27.7652	1.0249	9.8920	1.3169	
Peppers	5	0.4066	0.0807	0.9604	0.2109	2.9296	1.2273	0.6688	0.0469	0.4453	0.0200	1.0368	0.1599	<b>0.3718</b>	0.0866	28.4541	0.9821	22.1811	4.8004	
	2	0.5486	0.0320	0.6735	0.0663	1.9538	0.4469	0.6073	0.0373	0.3666	0.0113	1.0699	0.2502	<b>0.3175</b>	0.0597	28.3155	0.9546	1.9610	0.1213	
	3	0.4611	0.0198	0.7765	0.1908	2.0375	0.6774	0.6462	0.0418	0.3863	0.0081	1.4572	0.3676	<b>0.3554</b>	0.0512	29.0672	1.0098	7.5234	1.0287	
	4	0.4722	0.0052	0.6712	0.0548	2.4323	0.7498	0.6531	0.0557	<b>0.4104</b>	0.0117	1.6531	0.3279	0.4743	0.1582	29.2267	1.9326	19.8455	2.0641	
	5	<b>0.4554</b>	0.0471	0.7004	0.0700	2.6467	0.7098	0.6718	0.0550	0.4597	0.0462	1.4058	0.1300	0.5161	0.2231	29.1739	1.0126	17.9178	2.2472	
Livingroom	2	0.3637	0.0226	0.7587	0.1244	1.6007	0.1668	0.8707	0.5832	0.3673	0.0110	1.4021	0.2596	<b>0.3073</b>	0.0361	27.0961	1.1783	1.8237	0.1309	
	3	0.4088	0.0498	0.6675	0.0654	0.8836	0.5841	0.7755	0.2612	0.3976	0.0165	1.3682	0.2174	<b>0.3836</b>	0.1152	28.0109	1.1827	5.1459	0.5330	
	4	0.4140	0.0189	0.7090	0.0783	0.6984	0.2772	0.8185	0.1663	0.4127	0.0113	1.4302	0.2685	<b>0.3495</b>	0.0422	28.7899	1.2049	7.5004	1.2225	
	5	<b>0.4270</b>	0.0129	0.7047	0.0946	0.7076	0.1147	0.6885	0.0608	0.4455	0.0412	1.3652	0.0836	0.4290	0.0860	30.7696	1.7657	15.3806	3.9497	
	Barbara	2	0.4103	0.0302	0.6757	0.1135	0.4785	0.0334	0.7036	0.1103	0.3574	0.0126	1.3398	0.1636	<b>0.3124</b>	0.0353	28.2364	0.9413	3.2965	0.1628
Bridge	3	<b>0.3673</b>	0.0231	0.6619	0.1002	0.5340	0.0309	0.7693	0.1396	0.4215	0.0952	1.4771	0.2523	0.3869	0.0888	28.1234	1.1228	5.4275	0.5867	
	4	0.4399	0.1234	0.6949	0.1733	0.7640	0.1535	0.7226	0.0789	0.5638	0.0141	1.3984	0.0893	<b>0.3591</b>	0.0308	28.4611	1.0133	12.6877	1.8837	
	5	0.4105	0.1516	0.6434	0.0369	1.0049	0.0913	0.6963	0.0519	0.5969	0.3704	1.4842	0.1855	<b>0.4009</b>	0.1051	29.0858	0.9595	24.3296	2.7535	
	Barbara	2	0.4449	0.1109	0.6315	0.0562	0.7416	0.0693	0.7261	0.1710	0.3836	0.0234	1.7127	0.6467	<b>0.3103</b>	0.0329	27.9273	1.0859	2.0397	0.3205
	3	0.3923	0.0602	0.6312	0.0582	0.8086	0.0504	0.7352	0.1075	0.3967	0.0181	1.9683	0.4157	<b>0.3618</b>	0.0616	28.9527	1.2931	5.2253	0.6045	
Butterfly	4	0.5264	0.2399	0.6405	0.0349	0.8643	0.0710	0.8594	0.0935	0.4135	0.0091	2.1053	0.7307	<b>0.3774</b>	0.0585	28.8173	1.1539	12.3139	1.5128	
	5	<b>0.4008</b>	0.0949	0.7974	0.2033	1.0372	0.0782	0.8717	0.2213	0.4254	0.0086	1.7569	0.5571	0.4017	0.0461	29.1017	0.9857	22.1631	3.3969	
	Bridge	2	0.3754	0.0096	0.8044	0.2702	0.7379	0.0578	0.6565	0.0562	0.3723	0.0146	1.4086	0.0979	<b>0.3521</b>	0.1161	28.1295	1.2163	2.6121	0.1574
	3	0.4021	0.0098	0.9520	0.3040	0.8507	0.0819	0.7845	0.1938	0.3932	0.0135	1.4111	0.0859	<b>0.3487</b>	0.0657	29.3385	1.0648	6.3863	1.1067	
	4	<b>0.3142</b>	0.0120	0.8417	0.1274	0.9888	0.1273	0.7190	0.1190	0.4075	0.0087	1.4362	0.0702	0.3828	0.0808	29.4883	1.3169	13.0902	1.8122	
Lake	5	<b>0.4119</b>	0.0191	1.1483	0.4777	1.0253	0.1168	0.4609	0.0822	0.4239	0.0075	1.4656	0.1252	0.4203	0.0692	30.9883	1.0545	17.4014	2.1007	
	2	0.3471	0.0371	0.8747	0.3195	0.4462	0.0854	0.4709	0.0848	0.3749	0.0140	1.2632	0.0534	<b>0.3035</b>	0.0269	29.2435	2.2596	2.3037	0.1596	
	3	0.3635	0.0263	0.7099	0.0790	0.5040	0.1637	0.5451	0.1044	0.3947	0.0141	1.2667	0.0707	<b>0.3218</b>	0.0311	30.7816	3.3802	6.2413	0.5793	
	4	0.3811	0.0514	0.8566	0.3466	0.6021	0.2227	0.7175	0.1375	0.4169	0.0267	1.3410	0.0911	<b>0.3418</b>	0.0245	30.4488	1.2458	8.5249	0.9669	
	5	0.3942	0.0217	1.2632	0.4282	0.6891	0.1865	0.7661	0.1034	0.4352	0.0235	1.4830	0.3849	<b>0.3666</b>	0.0276	30.7334	0.9481	18.3921	3.3804	
Lake	2	0.3498	0.0163	0.9614	0.2589	0.3394	0.0322	0.6812	0.1123	0.3711	0.0129	2.0181	1.0256	<b>0.2981</b>	0.0360	28.3338	1.2955	1.4661	0.1355	
	3	<b>0.3110</b>	0.0220	0.9104	0.3963	0.3939	0.0194	0.8624	0.1749	0.4103	0.0461	2.65737	0.9526	0.3285	0.0241	30.3101	5.5916	6.0846	0.6608	
	4	0.3813	0.0075	0.6438	0.0704	0.4258	0.0196	0.9281	0.3201	0.4378	0.0518	1.9319	0.5351	<b>0.3510</b>	0.0385	30.0289	1.0629	9.1697	1.8032	
	5	0.3857	0.0535	0.7743	0.1485	0.9459	0.7620	0.7706	0.1164	0.4635	0.0619	1.7971	0.3117	<b>0.3757</b>	0.0602	30.6095	0.9276	17.8694	1.6750	

**Table 10**

Results after applying MCET-HHO to the set of benchmark images.



As it is possible to observe, the HHO and ABC images present precisely the same behavior, obtaining significant results, especially in the Cameraman, Lena, Jetplane, Living room, Bridge, and Lake images. The PSO and DE algorithms also show significant performance in these images. However, they do not exceed the results of the algorithms mentioned above.

On the other hand, the FFO algorithm is the only one that has a significant FFSIM value in Baboon, Pirate, and Butterfly images, while the HHO algorithm presents the best results for Jetplane, Peppers and Barbara images. The SCA algorithm does not show a significant performance for any of the images. In the case of the K-means and the Fuzzy IterAg algorithms, both present very similar

**Table 11**

Results after applying MCET-HHO to the set of benchmark images.

Image	nTh = 2	nTh = 3	nTh = 4	nTh = 5
Pirate				
Jetplane				
Peppers				

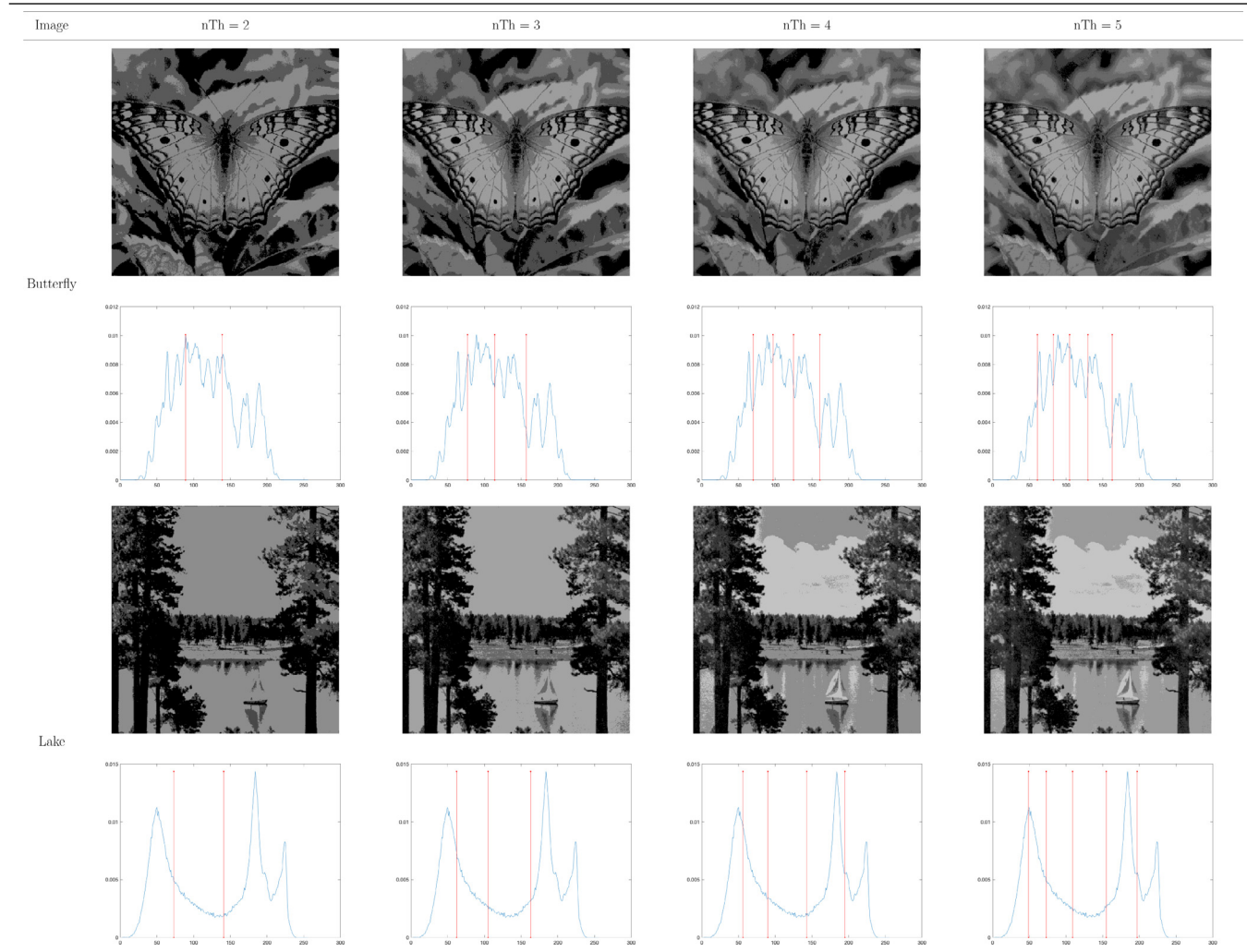
**Table 12**

Results after applying MCET-HHO to the set of benchmark images.

Image	nTh = 2	nTh = 3	nTh = 4	nTh = 5
Livingroom				
Barbara				
Bridge				

**Table 13**

Results after applying MCET-HHO to the set of benchmark images.



results, which are near to the average values presented by the rest of the algorithms, however, neither present any value that is the best among the other results.

Therefore, based on this metric, most of the algorithms, except for the SCA algorithm, present similar results on average, although the behavior is very variable between the images, since, as shown, the algorithms HHO, PSO, DE, HS, and ABC have similar quality of the segmentation for the same images, while the FFO algorithm presents a positive quality for different images, being evident that the distribution of gray levels affects the behavior of the algorithms.

In Table 9 is presented a comparison of the computational time calculated in seconds for each of the algorithms through the segmentation applied to the images using the four different levels. As it is possible to observe, in most cases the shortest time was obtained using the SCA algorithm; while for some of the levels of certain images, the HHO and HS algorithms presented the shortest time compared to the others; however, in general, computational times have very little difference between these three algorithms. In the case of the PSO, FFO, and DE algorithms, the times are slightly increased compared to the previous algorithms, while in the ABC algorithm, the time can be increased twice or triple. On the other hand, the difference of the K-means and Fuzzy IterAg algorithms can stand out significantly, since the computational times increase

up to 50 times or sometimes even more, compared to the algorithms that obtained the shortest times.

Therefore, based on computational time, the most efficient algorithms are SCA, HHO, and HS, while the K-means and Fuzzy IterAg algorithms have a significant deficiency. It is important to highlight this point taking into account that the algorithms that present the best computational times show a significant performance in the segmentation of the images according to the results of the evaluation metrics obtained, while the algorithms that present the worst times are also those that, if they do not show a much less significant performance, they also do not show the best results compared to the other algorithms.

Finally, Tables 10, 11, 12, and 13 presented the benchmark images after applying a segmentation based on a MCET-HHO approach using the four different levels,  $nTh = 2, 3, 4$  and  $5$ , in conjunction with their corresponding histogram, where the different thresholds selected by the algorithm are marked through a red vertical line.

As it is possible to observe, some images can be identified in which an improvement in the quality of their contrast is evident as the number of thresholds increases, especially in the images Cameraman, Lena, Pirate, Jetplane, Living room, Bridge, Butterfly, and Lake, showing a higher amount of details in the image with the highest amount of thresholds if it is compared with the image that only has two.

On the other hand, there are some images in which a significant improvement can also be observed while increasing the number of thresholds; however, when comparing the last two levels, where there are four and five thresholds, it is not possible to notice a significant change, as in the Barbara and Peppers images, so it could be enough to only have 4 thresholds to achieve an adequate quality in the image, allowing to observe the details of it. This may be because the original images probably do not have many details, as is the case with Peppers, or because the location of the thresholds based on the MCET-HHO algorithm is in a region of the histogram where there is no a significant change in gray levels between one threshold and the other, as in the case of Barbara, where the first two thresholds have very similar gray levels.

In the case of the Baboon image, it can be observed that the contrast improvement can be achieved from level 2, with three thresholds, since it is not possible to observe obvious changes by adding more thresholds. This may be because large numbers of pixels are located in the same region of the histogram, so that the gray levels contained in the different thresholds can be very similar, being unnecessary to be at a different level when having very similar information.

Therefore, based on the results of the previous metrics calculated, the values obtained can be understood, where the HHO algorithm shows its best average behavior in the images Cameraman, Lena, Jetplane, Living room, Bridge and Lake, being the majority of the images that present the greatest amount of detail, with a greater heterogeneity in their gray levels, according to their histograms, in addition to being distributed in a way that covers a greater amount of intensities, thus achieving a better quality in the segmentation by being able to differentiate with greater evidence between the different thresholds.

**Table 14** presents the p-values obtained from the Wilcoxon test, which are calculated by the comparison of the best value in terms of the MCET and PSNR between the algorithm HHO and each of the algorithms included, presenting six different pairs, PSO vs HHO, FFO vs HHO, DE vs HHO, HS vs HHO, ABC vs HHO and SCA vs HHO. Here is important to mention that the K-means and Fuzzy IterAg are not considered in this test due they are not metaheuristics, and their outputs do not change. When these p-values are lower than 0.05 allow them to know that they are statistically significant, since the null hypothesis is rejected, meaning that the methods compared present significant differences between each other. In order to simplify the interpretation of these values, the symbols ▲, ▶ and ▼ are included, representing the performance of the HHO algorithm against the compared technique based on improvement, no difference and worsening, respectively. According to this table, in most cases, a value lower than 0.05 is obtained for each pair of algorithms in the MCET and PSNR, showing a significant difference between the methods, especially in comparison with the FFO and SCA algorithms, where the MCET presents the lowest values for each of the levels applied to the benchmark images, while the PSNR allows observing better results in the comparison with the SCA than with the FFO. Based on the symbols accompanying each value, a significant improvement is shown by the HHO algorithm in the MCET, except only two values that are obtained from levels 4 and 5 of two different images, where worsening is shown, while in the SCA algorithm all levels an improvement for each image is observed. For the PSNR, the HHO algorithm presents a better improvement in the SCA than in the FFO, where the HHO improves only for some specific images. In the case of the comparison with the algorithms PSO, DE, HS, and ABC, the difference between the pairs in the MCET is less evident, showing several NaN's, representing that there is no difference between the methods. However, it can be noted that for most images, where there is a more significant difference is in the last levels, 3, 4, and 5, besides showing an improvement. According to the PSNR, the p-values obtained are

not usually significant in many cases, presenting a similar behavior for this metric in the different algorithms and the proposed one. The improvement for this metric is shown mainly at levels 4 and 5 in some images.

## 6.2. Experiments with the Berkeley dataset

The second set of images used to determine the performance of the MCET-HHO is applied to the Berkeley dataset for image segmentation. **Table 15** presents the results obtained through the application of the algorithms HHO, K-means, and Fuzzy IterAg to the 300 images of the Berkeley dataset, calculating the average of three different metrics, PRI, GCE, and Vol, to evaluate and compare the performance of these algorithms in the segmentation.

The PRI value allows to know the similarity between two groups of data. A higher value of this metric represents a better result, so it can be seen in the **Table 15** that the proposed algorithm has the highest average values. While the K-means and Fuzzy IterAg algorithms have lower values, demonstrating that the MCET-HHO algorithm exhibits better behavior segmented images.

In the case of the GCE value, it allows to measures the extent to which segmentation can be seen as a refinement of the other. The segmentations which are related are considered to be consistent since they could represent the same image segmented at different scales. A lower value of this metric represents better performance, and the Fuzzy IterAg algorithm presents better results.

Finally, the Vol metric allows the measurement of the distance between two clusterings and also, a lower value represents better performance. The best results are presented by the MCET-HHO approach, while the K-means and Fuzzy IterAg algorithms have similar values.

These metrics allow to demonstrate that the segmentation performed by the MCET-HHO approach is superior in comparisons with the other two state-of-the-art algorithms.

**Table 16** shows graphical examples using the second test of the Berkeley segmentation dataset provided by the MCET-HHO, K-means and Fuzzy IterAg algorithms. The images of the segmentation edges of the algorithms are presented in green, the ground-truth of the manual segmentation of the database in red and the match of the algorithm and the ground-truth in yellow. As it can be seen in the **Table 16**, the proposed MCET-HHO algorithm has more yellow contours, which means that it has better results in the segmentation of the images by comparing it against the others algorithms.

## 6.3. Experiments with digital mammograms

The third set of images used to determine the performance of the MCET-HHO applied to medical images, specifically mammography images, is presented in **Fig. 4**. Each of these images corresponds to a different a case.

It is important to mention that these images have been chosen because a potential application that could be given to this algorithm is the segmentation on mammography images for the automatic identification of different masses, such as breast tumors.

**Table 17** presents the results obtained through the application of the algorithms MCET-HHO, K-means, and Fuzzy IterAg to the mammography images, calculating the average of three different metrics, PSNR, SSIM, and FSIM, to evaluate and compare the performance of these algorithms.

In the case of the PSNR value, which allows to know the affinity between the original image and the image after the application of the algorithm where a higher value represents a better result, it is evident that the MCET-HHO has the highest values for all images applying the different levels, which corresponds to that the affinity between the images is better, while the other two algorithms have

**Table 14**

Comparison of the p-values obtained through the Wilcoxon signed-rank test between the pairs of PSO vs HHO, FFO vs HHO, DE vs HHO, HS vs HHO, ABC vs HHO and SCA vs HHO, for MCET and PSNR.

Image	nTh	PSO		FFO		DE		HS		ABC		SCA					
		MCET	PSNR	MCET	PSNR	MCET	PSNR	MCET	PSNR	MCET	PSNR	MCET	PSNR				
Cameraman	2	NaN	►	NaN	►	4.14E-14	▲	0.0265	▲	NaN	►	NaN	►	2.60E-11	▲	0.4940	▲
	3	NaN	►	NaN	►	2.11E-13	▲	0.2683	▼	NaN	►	NaN	►	1.53E-14	▲	0.2746	▲
	4	NaN	►	NaN	►	1.53E-14	▲	3.06E-5	▲	NaN	►	3.40E-5	►	0.3313	►	0.3313	►
	5	0.5692	▲	0.5692	►	2.18E-14	▲	4.60E-3	▲	1	▲	0.1664	▼	1.44E-3	▲	0.6470	►
Lena	2	NaN	►	NaN	►	1.03E-7	►	1.66E-5	▲	NaN	►	NaN	►	0.0423	▲	0.0423	▲
	3	NaN	►	NaN	►	1.50E-14	▲	0.8309	▲	NaN	►	NaN	►	0.0219	▲	0.0219	►
	4	1.63E-4	▲	1.63E-4	▲	1.53E-14	▲	4.36E-3	▲	1.79E-5	▲	2.02E-4	▲	4.13E-7	▲	4.13E-7	▲
	5	0.0220	▲	0.0220	▲	1.53E-14	▲	0.1255	▲	2.12E-13	▲	2.70E-8	▲	1.90E-9	▲	3.29E-8	▲
Baboon	2	NaN	►	NaN	►	1.59E-13	▲	0.5060	▲	NaN	►	NaN	►	NaN	►	NaN	►
	3	0.3313	▲	0.3313	►	2.09E-13	▲	2.39E-5	▼	NaN	►	NaN	►	0.0219	▲	0.0219	►
	4	NaN	►	NaN	►	1.53E-14	▲	0.8309	▼	0.0424	▲	0.0424	▲	1.63E-5	▲	1.63E-5	►
	5	0.0114	▲	0.0114	▼	1.53E-14	▲	4.36E-3	▼	2.52E-10	▲	0.8197	▲	6.63E-13	▲	0.3719	▲
Pirate	2	NaN	►	NaN	►	1.89E-13	▲	0.5073	▼	NaN	►	NaN	►	NaN	►	NaN	►
	3	NaN	►	NaN	►	5.79E-14	▲	0.6628	▼	NaN	►	NaN	►	0.3313	▲	0.3313	►
	4	0.9883	▲	0.9883	▼	3.65E-14	▲	0.8620	▼	0.3768	▲	0.3768	▼	1.22E-11	▲	1.22E-11	▼
	5	NaN	►	NaN	►	1.53E-14	▲	0.2746	▼	2.09E-9	▲	2.09E-9	▼	1.53E-14	▲	1.53E-14	►
Jetplane	2	NaN	►	NaN	►	6.23E-13	▲	7.62E-7	▲	NaN	►	NaN	►	NaN	►	NaN	►
	3	NaN	►	NaN	►	1.92E-13	▲	2.32E-5	▼	0.0227	▲	0.6546	▼	0.0114	▲	1	▼
	4	2.64E-6	▲	2.64E-6	▼	5.75E-14	▲	0.0778	▼	2.54E-12	▲	0.2611	▲	3.53E-8	▲	6.51E-6	▼
	5	8.15E-5	▲	8.61E-4	▼	1.53E-14	▲	0.0159	▲	1.53E-14	▲	0.5137	▼	1.37E-8	▲	1.34E-3	▼
Peppers	2	NaN	►	NaN	►	5.42E-13	▲	4.61E-9	▼	NaN	►	NaN	►	NaN	►	NaN	►
	3	0.0816	▲	0.0816	▼	1.52E-14	▲	0.2745	▼	5.89E-3	▲	5.89E-3	▼	4.64E-11	▲	9.89E-10	▼
	4	NaN	►	NaN	►	1.53E-14	▲	0.2746	▼	NaN	►	NaN	►	NaN	►	7.21E-10	►
	5	0.6221	▲	0.6221	▼	3.74E-8	▼	0.7095	▲	8.77E-3	▲	0.1582	▼	2.12E-9	▲	5.20E-7	▼
Living room	2	NaN	►	NaN	►	5.37E-13	▲	6.89E-3	▲	NaN	►	NaN	►	NaN	►	NaN	►
	3	NaN	►	NaN	►	1.52E-14	▲	1.00E-3	▼	NaN	►	NaN	►	NaN	►	NaN	►
	4	0.0113	▲	0.0113	▲	1.53E-14	▲	3.05E-5	▲	NaN	►	NaN	►	2.94E-3	▲	2.94E-3	▲
	5	NaN	►	NaN	►	1.53E-14	▲	1.93E-10	▲	0.1602	▲	1	▲	4.63E-12	▲	3.97E-7	▲
Barbara	2	0.1602	▲	0.1602	▼	1.97E-13	▲	2.93E-6	▼	NaN	►	NaN	►	NaN	►	NaN	►
	3	NaN	►	NaN	►	5.79E-14	▲	0.3798	▼	0.0220	▲	0.1713	▼	NaN	►	0.0423	▲
	4	1	▼	1	▲	3.40E-13	▼	2.41E-3	▼	6.88E-11	▼	0.3905	▼	0.3313	▼	0.3313	▲
	5	5.89E-3	▲	0.0495	▲	1.53E-14	▲	0.0159	▼	1.53E-14	▲	0.0486	▲	5.77E-9	▲	0.0528	▲
Bridge	2	NaN	►	NaN	►	5.61E-14	▲	9.91E-6	▲	NaN	►	NaN	►	NaN	►	NaN	►
	3	NaN	►	NaN	►	1.42E-14	▲	3.04E-9	▲	NaN	►	NaN	►	0.0220	▲	0.1712	▲
	4	0.0242	▲	0.5469	▲	2.57E-13	▲	7.59E-13	▲	0.7950	▲	6.023E-3	▼	4.41E-10	▲	0.7131	▲
	5	1.05E-6	▲	0.7111	▼	1.00E-12	▲	0.1495	▲	0.0423	▼	0.0329	▼	0.0578	▲	0.6428	▲
Butterfly	2	NaN	►	NaN	►	5.40E-10	▲	8.40E-4	▼	0.3313	▲	0.3313	▲	2.97E-3	▲	0.0260	▼
	3	0.3313	▲	0.3313	▲	5.64E-14	▲	8.08E-3	▼	0.0817	▲	0.0817	▲	0.0219	▲	0.1602	▲
	4	0.0113	▲	0.0113	▼	1.53E-14	▲	3.06E-5	▼	8.40E-12	▲	1.44E-3	▼	0.0113	▲	2.68E-11	▲
	5	1.78E-5	▲	1.78E-5	▲	1.53E-14	▲	0.8309	▲	1.53E-14	▲	0.0159	▲	8.31E-12	▲	8.31E-12	▲
Lake	2	NaN	►	NaN	►	4.53E-13	▲	6.71E-3	▲	NaN	►	NaN	►	NaN	►	NaN	►
	3	NaN	►	NaN	►	8.34E-12	▲	0.1734	▼	NaN	►	NaN	►	1.84E-9	▲	1.79E-3	▼
	4	0.0423	▲	0.0423	▲	1.53E-14	▲	0.0159	▲	NaN	►	NaN	►	5.86E-10	▲	5.86E-10	▲
	5	0.0114	▲	0.0924	▼	1.52E-14	▲	0.8309	▲	1.79E-5	▲	0.1543	▲	1.96E-13	▲	0.1200	▲

**Table 15**

Comparison of PRI, GCE and Vol values obtained with MCET-HHO, K-means and Fuzzy IterAg in the Berkeley dataset.

HHO						K-means						Fuzzy IterAg						
PRI		GCE		Vol		PRI		GCE		Vol		PRI		GCE		Vol		
Mean	Std	Mean	Std	Mean	Std	Mean	Std	Mean	Std	Mean	Std	Mean	Std	Mean	Std	Mean	Std	
Total	<b>0.8992</b>	0.0348	0.0327	0.0151	<b>0.3568</b>	0.0996	0.8973	0.0355	0.0327	0.0149	0.3594	0.0998	0.8982	0.0332	<b>0.0321</b>	0.0145	0.3573	0.0936

**Table 16**

Results after applying MCET-HHO, K-means and Fuzzy IterAg to the Berkeley segmentation dataset.

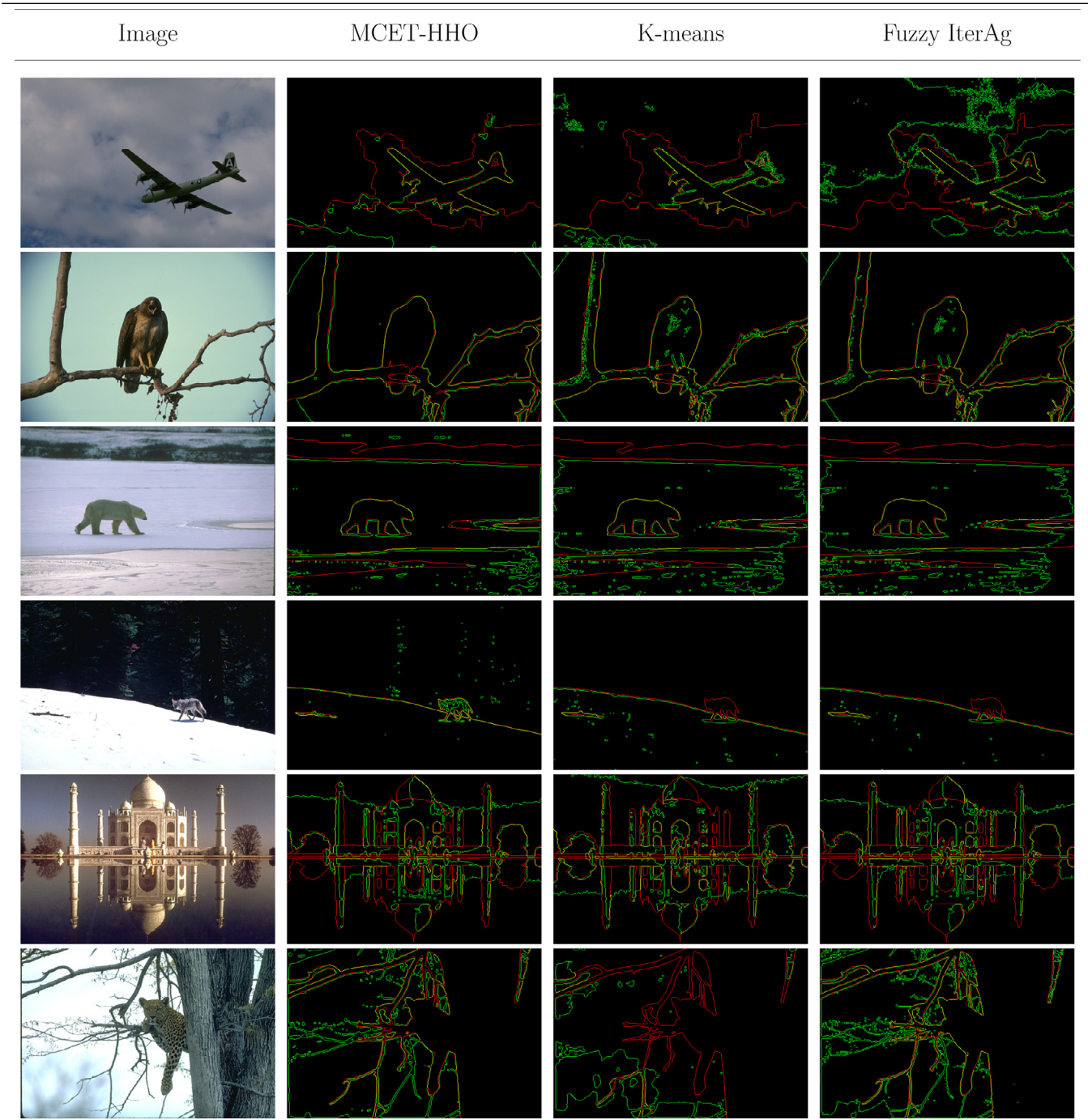


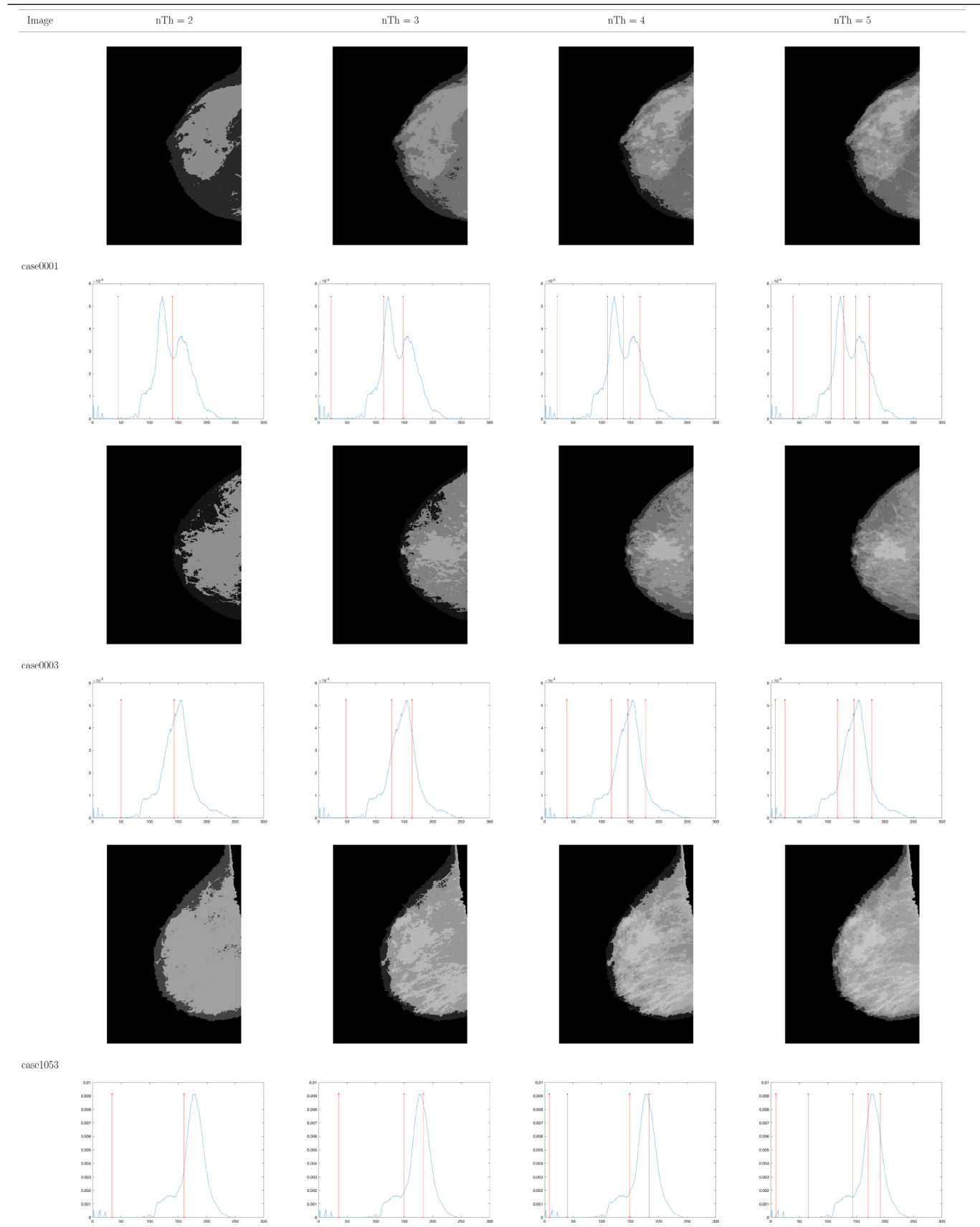
**Table 17**

Comparison of PSNR, SSIM and FSIM values obtained with HHO, K-means and Fuzzy IterAg in the set of digital mammograms.

Image	nTh	HHO						K-means						Fuzzy IterAg					
		PSNR		SSIM		FSIM		PSNR		SSIM		FSIM		PSNR		SSIM		FSIM	
		Mean	Std	Mean	Std	Mean	Std	Mean	Std	Mean	Std	Mean	Std	Mean	Std	Mean	Std	Mean	Std
case0001	2	<b>17.4337</b>	0.9505	<b>0.8754</b>	0.0191	<b>0.9155</b>	0.0041	12.0747	2.1081	0.7394	0.0521	0.8987	0	10.5037	5.41E-15	0.7018	1.13E-16	0.8991	7.89E-16
	3	<b>23.2831</b>	1.0035	<b>0.9122</b>	0.0086	<b>0.9267</b>	0.0047	11.8696	3.3330	0.7253	0.0621	0.9031	0.0026	11.2515	3.60E-15	0.7133	4.51E-16	0.8896	0
	4	<b>24.8219</b>	1.2705	<b>0.9198</b>	0.0079	<b>0.9404</b>	0.0078	11.9326	2.7066	0.7380	0.0596	0.8909	0.0127	11.6931	9.01E-15	0.7234	3.38E-16	0.8891	5.63E-16
	5	<b>26.0339</b>	1.4279	<b>0.9246</b>	0.0073	<b>0.9514</b>	0.0084	12.2635	2.8534	0.7482	0.0663	0.8939	0.0161	14.3544	1.26E-14	0.7874	4.51E-16	0.9019	3.38E-16
	case0003	2	<b>18.4211</b>	0.9581	<b>0.8854</b>	0.0137	<b>0.9041</b>	0.0041	12.7711	2.1915	0.7741	0.0467	0.8851	0	10.4767	1.80E-15	0.7256	3.38E-16	0.8885
case1053	3	<b>21.8022</b>	0.8942	<b>0.9042</b>	0.0076	<b>0.9298</b>	0.0041	12.2848	3.7951	0.7566	0.0669	0.9130	0.0046	10.8792	3.60E-15	0.7317	4.51E-16	0.8715	5.63E-16
	4	<b>24.7044</b>	1.3159	<b>0.9207</b>	0.0079	<b>0.9466</b>	0.0062	11.6804	3.2146	0.7501	0.0569	0.9038	0.0179	11.5895	9.01E-15	0.7439	3.38E-16	0.8821	7.89E-16
	5	<b>26.1084</b>	1.1769	<b>0.9279</b>	0.0056	<b>0.9594</b>	0.0071	12.7156	2.9990	0.7812	0.0654	0.9022	0.0150	14.5452	1.80E-15	0.8070	3.38E-16	0.8913	3.38E-16
	2	<b>17.6829</b>	0.7053	<b>0.8689</b>	0.0087	<b>0.8307</b>	0.0036	10.7728	2.2116	0.6980	0.0648	0.7999	0	9.4161	7.21E-15	0.6526	5.63E-16	0.8022	6.76E-16
	3	<b>19.9762</b>	0.9584	<b>0.8701</b>	0.0094	<b>0.8844</b>	0.0179	9.2722	4.0082	0.6438	0.0952	0.8614	0.0052	17.0660	0	0.8459	3.38E-16	0.8543	6.76E-16
case3010	4	<b>21.5240</b>	1.0915	<b>0.8802</b>	0.0076	<b>0.9107</b>	0.0135	9.9160	3.9427	0.6692	0.0926	0.8289	0.0434	18.9761	7.21E-15	0.8443	5.63E-16	0.8812	6.76E-16
	5	<b>23.2889</b>	0.8935	<b>0.8942</b>	0.0049	<b>0.9317</b>	0.0054	11.2691	4.2694	0.7066	0.0957	0.8318	0.0420	20.2196	0.0354	0.8559	0.0005	0.9017	0.0008
	2	<b>17.4045</b>	0.7629	<b>0.8465</b>	0.0109	<b>0.7659</b>	0.0048	9.4787	2.6609	0.6297	0.0858	0.7374	2.27E-16	10.9979	3.60E-15	0.6768	3.38E-16	0.7371	2.25E-16
	3	<b>20.4886</b>	0.9682	<b>0.8289</b>	0.0089	<b>0.8517</b>	0.0079	11.9576	5.5575	0.6642	0.1347	0.8137	0.0039	17.9091	7.21E-15	0.7891	4.51E-16	0.8156	4.51E-16
	4	<b>22.3842</b>	1.2910	<b>0.8510</b>	0.0128	<b>0.8837</b>	0.0180	11.4103	5.3174	0.6574	0.1134	0.7805	0.0589	20.4010	7.21E-15	0.8238	3.38E-16	0.8549	0
case3018	5	<b>23.9218</b>	1.1576	<b>0.8675</b>	0.0092	<b>0.9081</b>	0.0143	10.4346	4.0881	0.6464	0.0880	0.7528	0.0489	23.2365	1.80E-14	0.8502	5.63E-16	0.8898	9.01E-16
	2	<b>15.5205</b>	0.9882	<b>0.7540</b>	0.0267	<b>0.7745</b>	0.0098	11.0271	1.9019	0.5871	0.0817	0.7332	3.40E-16	8.6982	1.80E-15	0.4808	5.63E-17	0.7292	3.38E-16
	3	<b>21.3253</b>	1.3118	<b>0.8376</b>	0.0158	<b>0.8290</b>	0.0126	13.0901	4.7367	0.6276	0.1572	0.7828	0.0063	10.8208	3.60E-15	0.5773	0	0.7437	5.63E-16
	4	<b>23.3559</b>	1.3703	<b>0.8537</b>	0.0119	<b>0.8747</b>	0.0210	14.8385	5.6521	0.6788	0.1418	0.7920	0.0523	15.5190	9.01E-15	0.7228	1.13E-16	0.7716	3.38E-16
	5	<b>24.3471</b>	1.0658	<b>0.8639</b>	0.0091	<b>0.8963</b>	0.0129	14.4071	4.5853	0.6919	0.1176	0.7812	0.0502	18.5784	7.21E-15	0.7944	4.51E-16	0.8081	7.89E-16
case3020	2	<b>13.4547</b>	0.6802	<b>0.7617</b>	0.0358	<b>0.8001</b>	0.0048	10.3849	1.7251	0.5546	0.0742	0.7349	0.0079	10.0641	1.80E-15	0.5334	3.38E-16	0.7527	3.38E-16
	3	<b>15.8408</b>	0.8403	<b>0.7986</b>	0.0308	<b>0.8125</b>	0.0073	12.5129	2.8481	0.6334	0.1107	0.7471	0.0136	10.6148	5.41E-15	0.5497	0	0.7330	6.76E-16
	4	<b>16.8728</b>	0.9678	<b>0.8076</b>	0.0296	<b>0.8416</b>	0.0100	12.5588	4.6422	0.6304	0.1466	0.7575	0.0354	11.4809	0	0.5839	3.38E-16	0.7405	0
	5	<b>23.6979</b>	2.4505	<b>0.8842</b>	0.0257	<b>0.8687</b>	0.0117	13.2903	3.8048	0.6952	0.1070	0.7543	0.03745	11.7368	7.21E-15	0.5905	1.13E-16	0.7479	5.63E-16
	2	<b>14.2158</b>	0.8007	<b>0.7535</b>	0.0336	<b>0.7836</b>	0.0067	11.1918	1.7738	0.5887	0.0658	0.7326	0.0019	10.1194	5.41E-15	0.5433	1.13E-16	0.7333	3.38E-16
case3050	3	<b>18.4619</b>	0.8648	<b>0.8144</b>	0.0186	<b>0.8160</b>	0.0088	11.7448	3.7182	0.6003	0.1266	0.7750	0.0073	11.2268	5.41E-15	0.5870	3.38E-16	0.7475	2.25E-16
	4	<b>20.2104</b>	1.0674	<b>0.8331</b>	0.0179	<b>0.8496</b>	0.0109	11.6010	3.5114	0.6221	0.1154	0.7682	0.0251	12.8486	7.21E-15	0.6338	4.51E-16	0.7538	4.51E-16
	5	<b>21.3886</b>	0.6709	<b>0.8466</b>	0.0089	<b>0.8687</b>	0.0076	14.0278	3.7062	0.7194	0.1029	0.7893	0.0311	13.8020	9.01E-15	0.6629	3.38E-16	0.7720	4.51E-16
	2	<b>13.2405</b>	0.8278	<b>0.7859</b>	0.0298	<b>0.8054</b>	0.0056	9.8043	1.6401	0.6287	0.0604	0.7592	0	9.5909	5.41E-15	0.6232	0	0.7572	1.13E-16
	3	<b>21.1066</b>	0.8278	<b>0.8753</b>	0.0086	<b>0.8324</b>	0.0069	10.9852	3.9047	0.6453	0.1113	0.7804	0.0091	10.6178	3.60E-15	0.6533	2.25E-16	0.7710	3.38E-16
case3057	4	<b>23.2326</b>	0.9785	<b>0.8782</b>	0.0067	<b>0.8860</b>	0.0149	9.9193	3.9474	0.6247	0.1035	0.7851	0.0448	17.0789	0	0.8093	5.63E-16	0.8054	4.51E-16
	5	<b>24.3452</b>	1.0082	<b>0.8812</b>	0.0061	<b>0.9114</b>	0.0120	12.5173	4.2326	0.7139	0.0974	0.7894	0.0465	20.5441	7.21E-15	0.8594	5.63E-16	0.8466	3.38E-16

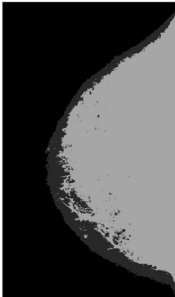
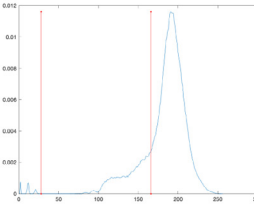
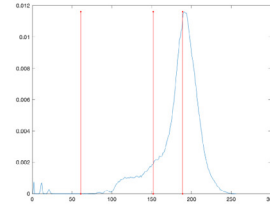
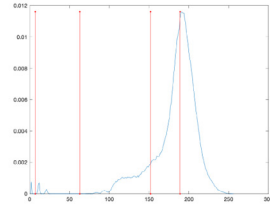
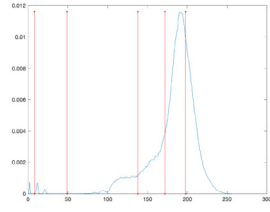
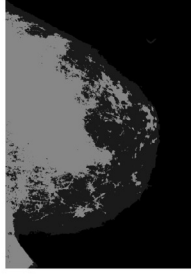
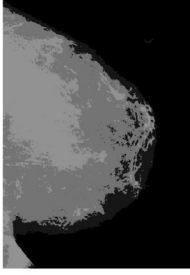
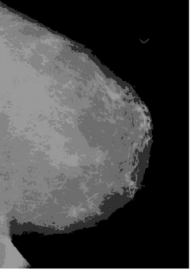
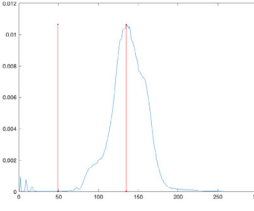
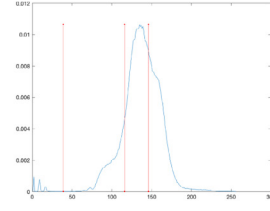
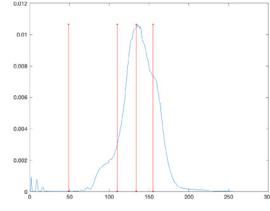
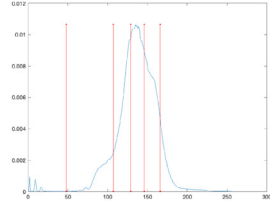
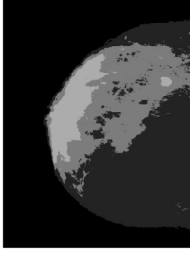
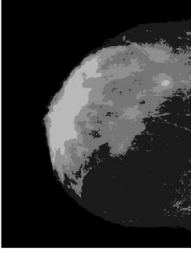
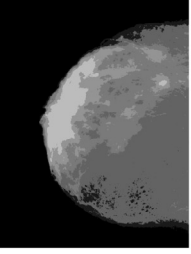
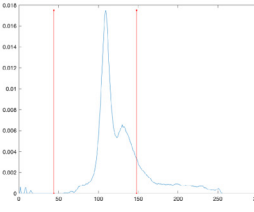
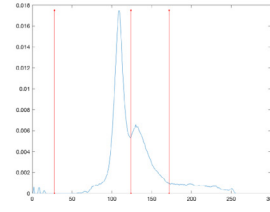
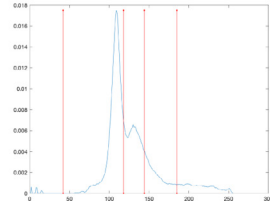
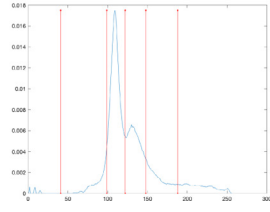
**Table 18**

Results after applying MCET-HHO to the set of digital mammograms.



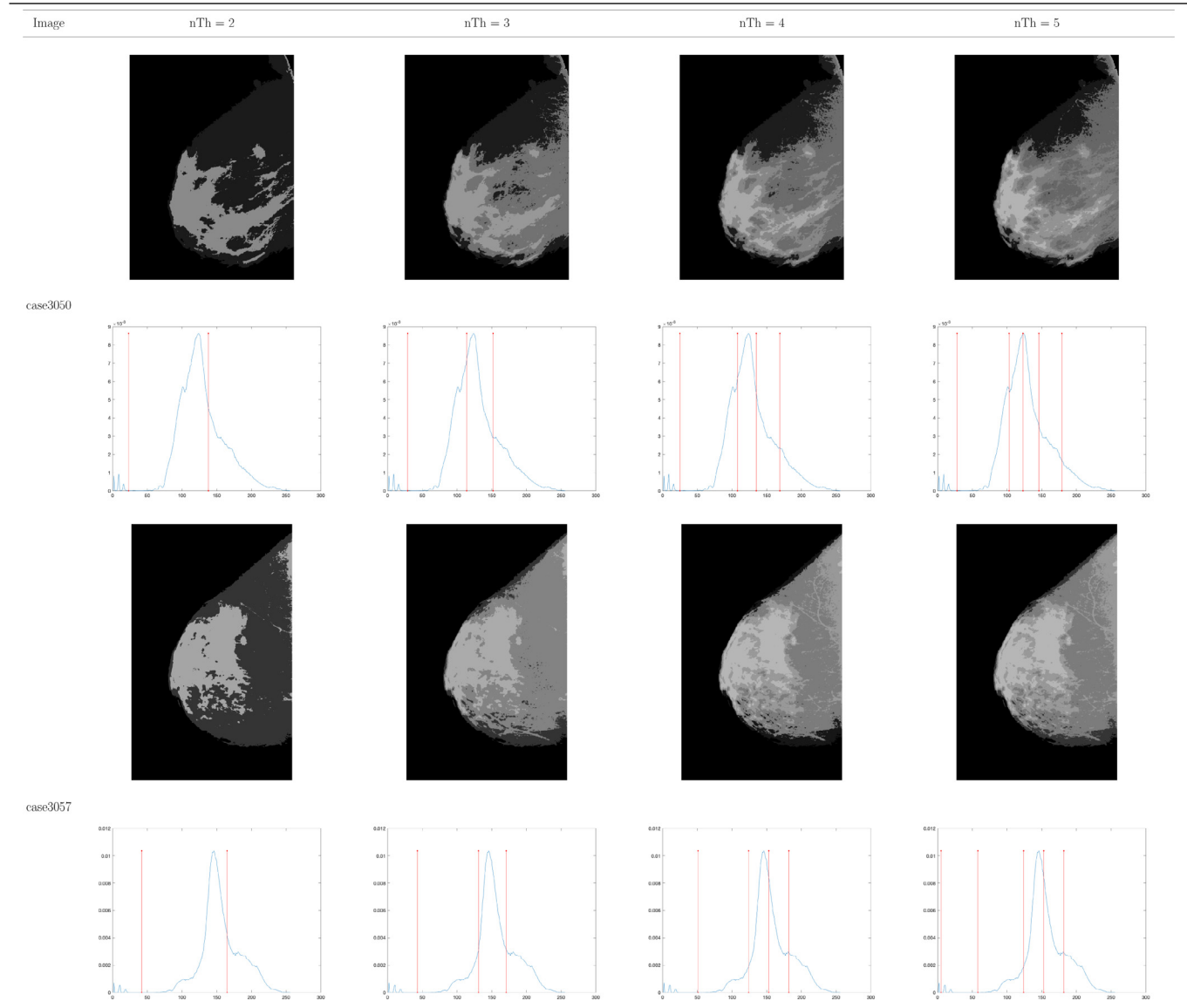
**Table 19**

Results after applying MCET-HHO to set of digital mammograms.

Image	nTh = 2	nTh = 3	nTh = 4	nTh = 5
				
case3010				
				
case3018				
				
case3020				

**Table 20**

Results after applying MCET-HHO to the set of digital mammograms.



significantly lower values, demonstrating that the MCET-HHO algorithm has a better behavior when segmenting these images based on its multilevel approach.

The SSIM value, which allows comparing the structures within the segmented image and a higher value represents better performance, also presents the best results for the MCET-HHO for all images, while the K-means and Fuzzy IterAg algorithms continue presenting results that do not exceed those obtained by the MCET-HHO. This allows to know that the algorithm that best compares structures in the image, making reference to the fact that segmentation is better, is MCET-HHO.

Finally, for the FSIM index, which allows measuring the quality of the segmentation and in the same way a higher value represents better performance, the best results are presented by the MCET-HHO algorithm. The K-means and Fuzzy IterAg algorithms generally have very similar values and, although for some levels of the images they can also present similar values to those obtained by the MCET-HHO, mainly for levels 2 and 3, they remain with lower values. This allows to demonstrate that the segmen-

tion performed by the MCET-HHO algorithm using different levels has a better quality compared to the other two algorithms.

In Tables 18–20 are shown the results obtained through the application of the MCET-HHO algorithm to the mammography images using the four different levels,  $nTh = 2, 3, 4$  and  $5$ , in conjunction with their corresponding histogram, where the different thresholds selected by the algorithm are marked through a red vertical line. Here, it can be observed that each level allows to identify different regions of the breast more quickly than in the original images, since it allows to highlight the contrast of the details within the breast that generally could not be so evident because the gray levels can be very similar in the tissues of the breast, causing confusion in the interpretation of these images and even letting important details go unnoticed, such as the presence of malignant tumors.

Through these results, it is possible to observe that the MCET-HHO has a significant performance applied in mammography images, compared to other widely used algorithms, which could represent a potential application in the field of the enhancement of

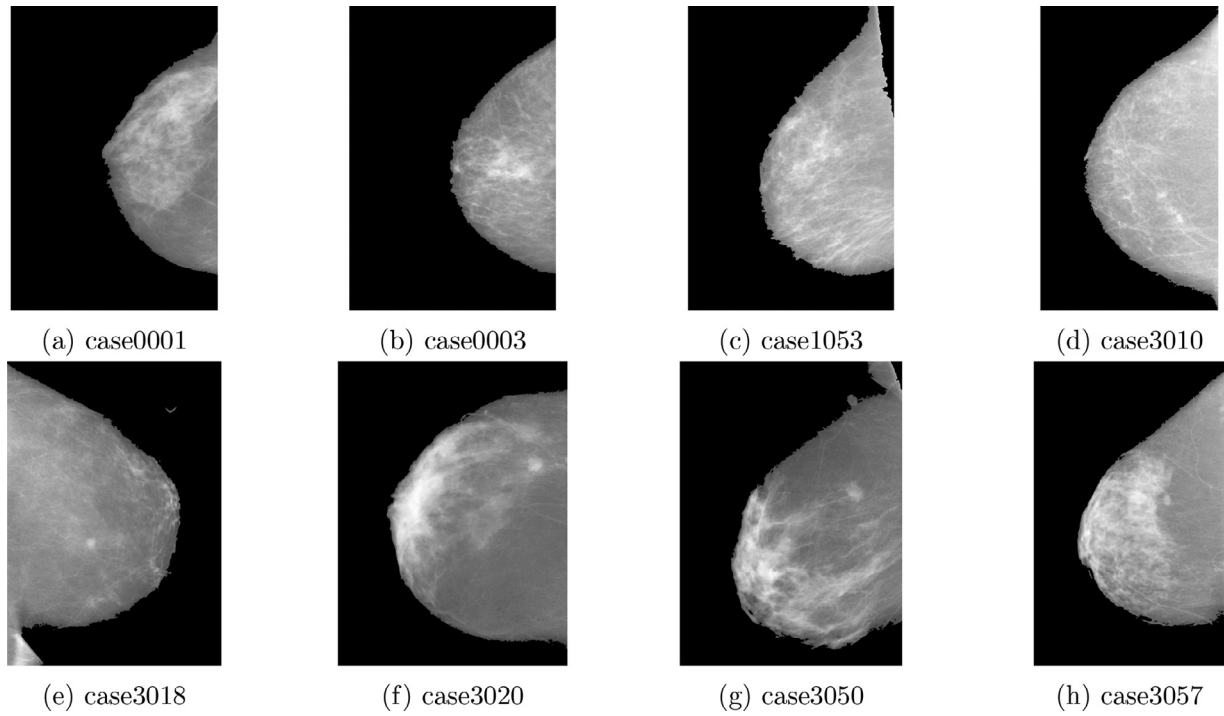


**Fig. 4.** Set of digital mammograms.

these medical images for different purposes, among them the identification of malignant tumors, as mentioned earlier, as well as the identification of benign tumors, calcifications, microcalcifications, among others, in order to improve the diagnosis of different conditions, such as breast cancer.

## 7. Conclusions and future works

This work proposes the application of a new approach based on the HHO metaheuristic algorithm for multilevel segmentation called MCET-HHO. The proposed method optimizes the search for the best solution of a function inspired by the behavior of the Harris hawks, based on the technique of the minimization of cross-entropy. For the development of this proposal, a comparison of the multilevel segmentation of three benchmarks is performed, one that presents images with different characteristics in the intensities of their gray levels, another in the Berkeley segmentation database, and finally in Medical images of digital mammograms. In order to validate the behavior of the MCET-HHO algorithm, the segmentation of the images is carried out with four different levels, obtaining a series of metrics that allow measuring the quality of the segmentation for each of the levels. In addition, the multilevel segmentation of these images is also carried out with a series of different algorithms, allowing the results obtained in this work to be compared with those currently found in the literature.

Based on the outcomes, it can be detected that the MCET-HHO presents significant results because according to the average values obtained based on the application of the cross entropy method for the different algorithms, the best values are presented mostly in the approach proposed, being important to take into account that despite using different threshold values, which depend on the level, and that the images also present heterogeneous values in their gray intensities. This algorithm presents robustness in its behavior. This robustness is reaffirmed through the metrics used for the validation of the results, where it is possible to identify the

images for which the best behavior of the MCET-HHO is presented compared to the other algorithms used. In addition to the optimal number of levels to be applied depending on the features of the gray intensities that can be observed through its histograms.

Therefore, it can be concluded that the MCET-HHO algorithm exhibits a better behavior if the amount of thresholds is consistent with the amount of image detail since it obviously allows segmenting while respecting essential descriptive regions of the image. Moreover, a better result is obtained if the distribution of gray levels within the histogram allows the identification of regions where there are groups of intensities and not so much a uniform distribution. Since the higher the change between one group of intensities and another, it will be easier to identify the location of a threshold, retaining important details that resemble the segmented image with the original, being difficult to identify the differences between both images.

Finally, the MCET-HHO algorithm shows an improvement in multilevel segmentation applied to images compared to the different algorithms reported in the literature included in this work, presenting a new approach that can be used for different applications as a complement to the different techniques that are currently used. The proposed approach is adequate to improve digital mammograms, as evidenced by the results. Since medical imaging is crucial for the diagnosis of many diseases, these topics have gained attention to researchers in recent years.

Although the results provide evidence that the proposed MCET-HHO method works well in all three tests performed, this document is not designed to devise a multilevel threshold method capable of exceeding all currently available methods, but to evaluate the HHO performance in real applications and not just reference problems. One of the main downsides is that the proposal is not automatic, and it is necessary to provide the number of thresholds to find. Moreover, in the current form, the proposed approach is not able to handle RGB images. For the future development of the proposal presented, it is intended to perform a comparison of

the optimization of other statistical criteria such as Otsu, Kapur, and Tsallis. Moreover, it is expected to combine it with reinforcement learning or machine learning to automatically search the best number of thresholds for a specific image. Finally, another research direction is to apply it for color images.

### Declaration of Competing Interest

None of the authors of this paper has a financial or personal relationship with other people or organizations that could inappropriately influence or bias the content of the paper.

It is to specifically state that "No Competing interests are at stake and there is No Conflict of Interest" with other people or organizations that could inappropriately influence or bias the content of the paper.

### Credit authorship contribution statement

**Erick Rodríguez-Esparza:** Conceptualization, Investigation, Methodology, Software, Writing - original draft. **Laura A. Zanella-Calzada:** Investigation, Methodology, Writing - original draft. **Diego Oliva:** Conceptualization, Investigation, Methodology, Writing - original draft. **Ali Asghar Heidari:** Methodology, Data curation, Validation. **Daniel Zaldivar:** Validation, Writing - review & editing. **Marco Pérez-Cisneros:** Validation, Writing - review & editing. **Loke Kok Foong:** Validation, Writing - review & editing.

### References

- Agrawal, S., Panda, R., Bhuyan, S., & Panigrahi, B. K. (2013). Tsallis entropy based optimal multilevel thresholding using cuckoo search algorithm. *Swarm and Evolutionary Computation*, 11, 16–30.
- Ahmadi, M., Kazemi, K., Aarabi, A., Niknam, T., & Helfroush, M. S. (2019). Image segmentation using multilevel thresholding based on modified bird mating optimization. *Multimedia Tools and Applications*, 1–25.
- Aja-Fernández, S., Curiale, A. H., & Vegas-Sánchez-Ferrero, G. (2015). A local fuzzy thresholding methodology for multiregion image segmentation. *Knowledge-Based Systems*, 83, 1–12.
- Aljarah, I., Mafarja, M., Heidari, A. A., Faris, H., & Mirjalili, S. (2020). Clustering analysis using a novel locality-informed grey wolf-inspired clustering approach. *Knowledge and Information Systems*, 62(2), 507–539.
- Arbelaez, P., Maire, M., Fowlkes, C., & Malik, J. (2011). Contour detection and hierarchical image segmentation. *IEEE Transactions on Pattern Analysis and Machine Intelligence*, 33(5), 898–916. doi:10.1109/TPAMI.2010.161.
- Avutu, S. K., Bajaj, V., Kumar, A., & Singh, G. K. (2019). A novel pectoral muscle segmentation from scanned mammograms using emo algorithm. *Biomedical Engineering Letters*, 9(4), 481–496.
- Chen, H., Heidari, A. A., Zhao, X., Zhang, L., & Chen, H. (2020a). Advanced orthogonal learning-driven multi-swarm sine cosine optimization: Framework and case studies. *Expert Systems with Applications*, 144, 113113.
- Chen, H., Jiao, S., Heidari, A. A., Wang, M., Chen, X., & Zhao, X. (2019a). An opposition-based sine cosine approach with local search for parameter estimation of photovoltaic models. *Energy Conversion and Management*, 195, 927–942.
- Chen, H., Jiao, S., Wang, M., Heidari, A. A., & Zhao, X. (2020b). Parameters identification of photovoltaic cells and modules using diversification-enriched harris hawks optimization with chaotic drifts. *Journal of Cleaner Production*, 244, 118778.
- Chen, H., Li, S., Heidari, A. A., Wang, P., Li, J., Yang, Y., ... Huang, C. (2020c). Efficient multi-population outpost fruit fly-driven optimizers: Framework and advances in support vector machines. *Expert Systems with Applications*, 142, 112999.
- Chen, H., Yang, C., Heidari, A. A., & Zhao, X. (2019b). An efficient double adaptive random spare reinforced whale optimization algorithm. *Expert Systems with Applications*, 113018.
- Chen, L.-C., Papandreou, G., Kokkinos, I., Murphy, K., & Yuille, A. L. (2017). Deeplab: Semantic image segmentation with deep convolutional nets, atrous convolution, and fully connected crfs. *IEEE Transactions on Pattern Analysis and Machine Intelligence*, 40(4), 834–848.
- Dorigo, M., & Di Caro, G. (1999). Ant colony optimization: a new meta-heuristic. In *Proceedings of the 1999 congress on evolutionary computation-cec99 (cat. no. 99th8406): 2* (pp. 1470–1477). IEEE.
- Eberhart, R., & Kennedy, J. (1995). A new optimizer using particle swarm theory. In *Mhs'95. proceedings of the sixth international symposium on micro machine and human science* (pp. 39–43). Ieee.
- Elaziz, M. A., Ewees, A. A., & Hassanien, A. E. (2017). Whale optimization algorithm and moth-flame optimization for multilevel thresholding image segmentation. *Expert Systems with Applications*, 83, 242–256.
- Elaziz, M. A., & Lu, S. (2019). Many-objectives multilevel thresholding image segmentation using knee evolutionary algorithm. *Expert Systems with Applications*, 125, 305–316.
- Elaziz, M. A., Oliva, D., Ewees, A. A., & Xiong, S. (2019). Multi-level thresholding-based grey scale image segmentation using multi-objective multi-verse optimizer. *Expert Systems with Applications*, 125, 112–129.
- Faris, H., Ala'M, Heidari, A. A., Aljarah, I., Mafarja, M., ... Fujita, H. (2019). An intelligent system for spam detection and identification of the most relevant features based on evolutionary random weight networks. *Information Fusion*, 48, 67–83.
- Faris, H., Heidari, A. A., Ala'M, A.-Z., Mafarja, M., Aljarah, I., Eshtay, M., & Mirjalili, S. (2020). Time-varying hierarchical chains of salps with random weight networks for feature selection. *Expert Systems with Applications*, 140, 112898.
- Faris, H., Mafarja, M. M., Heidari, A. A., Aljarah, I., Ala'M, A.-Z., Mirjalili, S., & Fujita, H. (2018). An efficient binary salp swarm algorithm with crossover scheme for feature selection problems. *Knowledge-Based Systems*, 154, 43–67.
- Formato, R. A. (2007). Central force optimization. *Prog Electromagn Res*, 77, 425–491.
- Gao, W., Guirao, J. L., Basavanagoud, B., & Wu, J. (2018a). Partial multi-dividing ontology learning algorithm. *Information Sciences*, 467, 35–58.
- Gao, W., Guirao, J. L. G., Abdel-Aty, M., & Xi, W. (2019). An independent set degree condition for fractional critical deleted graphs.. *Discrete & Continuous Dynamical Systems-Series S*, 12(4&5), 877–886.
- Gao, W., Wang, W., Dimitrov, D., & Wang, Y. (2018b). Nano properties analysis via fourth multiplicative abc indicator calculating. *Arabian Journal of Chemistry*, 11(6), 793–801.
- Gao, W., Wu, H., Siddiqui, M. K., & Baig, A. Q. (2018c). Study of biological networks using graph theory. *Saudi Journal of Biological Sciences*, 25(6), 1212–1219.
- Geem, Z. W., Kim, J. H., & Loganathan, G. V. (2001). A new heuristic optimization algorithm: Harmony search. *Simulation*, 76(2), 60–68.
- Ghamisi, P., Couceiro, M. S., & Benediktsson, J. A. (2012a). Extending the fractional order darwinian particle swarm optimization to segmentation of hyperspectral images. In *Image and signal processing for remote sensing xviii: 8537* (p. 85370F). International Society for Optics and Photonics.
- Ghamisi, P., Couceiro, M. S., Benediktsson, J. A., & Ferreira, N. M. (2012b). An efficient method for segmentation of images based on fractional calculus and natural selection. *Expert Systems with Applications*, 39(16), 12407–12417.
- He, L., & Huang, S. (2017). Modified firefly algorithm based multilevel thresholding for color image segmentation. *Neurocomputing*, 240, 152–174.
- Heath, M., Bowyer, K., Kopans, D., Moore, R., & Kegelmeyer, W. P. (2000). The digital database for screening mammography. In *Proceedings of the 5th international workshop on digital mammography* (pp. 212–218). Medical Physics Publishing.
- Heidari, A. A., Mirjalili, S., Faris, H., Aljarah, I., Mafarja, M., & Chen, H. (2019). Harris hawks optimization: Algorithm and applications. *Future Generation Computer Systems*, 97, 849–872.
- Hinojosa, S., Oliva, D., Cuevas, E., Pérez-Cisneros, M., & Pájares, G. (2018). Real-time video thresholding using evolutionary techniques and cross entropy. In *2018 ieee conference on evolving and adaptive intelligent systems (eais)* (pp. 1–8). IEEE.
- Holland, J. H. (1992). Genetic algorithms. *Scientific American*, 267(1), 66–73.
- Hore, A., & Ziou, D. (2010). Image quality metrics: Psnr vs. ssim. In *2010 20th international conference on pattern recognition* (pp. 2366–2369). IEEE.
- Hornig, M.-H., & Liou, R.-J. (2011). Multilevel minimum cross entropy threshold selection based on the firefly algorithm. *Expert Systems with Applications*, 38(12), 14805–14811.
- Huang, H., Heidari, A. A., Xu, Y., Wang, M., Liang, G., Chen, H., & Cai, X. (2020). Rationalized Sine Cosine Optimization with Efficient Searching Patterns (8, pp. 61471–61490). IEEE Access.
- Jinlong, L., Wenjie, X., Jianjing, Z., Wei, L., Xilin, S., & Chunhe, Y. (2020). Modeling the mining of energy storage salt caverns using a structural dynamic mesh. *Energy*, 193, 116730.
- Kapur, J. N., Sahoo, P. K., & Wong, A. K. (1985). A new method for gray-level picture thresholding using the entropy of the histogram. *Computer Vision, Graphics, and Image Processing*, 29(3), 273–285.
- Karaboga, D., & Basturk, B. (2007). A powerful and efficient algorithm for numerical function optimization: Artificial bee colony (abc) algorithm. *Journal of Global Optimization*, 39(3), 459–471.
- Kennedy, J. (2010). Particle swarm optimization. *Encyclopedia of Machine Learning*, 760–766.
- Khaled, A., Abdel-Kader, R. F., & Yasein, M. S. (2016). A hybrid color image quantization algorithm based on k-means and harmony search algorithms. *Applied Artificial Intelligence*, 30(4), 331–351.
- Koza, J. R., & Koza, J. R. (1992). *Genetic programming: On the programming of computers by means of natural selection*: 1. MIT press.
- Kullback, S. (1968). *Information theory and statistics*. Courier Corporation.
- Kumar, A. S., Kumar, A., Bajaj, V., & Singh, G. (2018). Fractional-order darwinian swarm intelligence inspired multilevel thresholding for mammogram segmentation. In *2018 international conference on communication and signal processing (iccsip)* (pp. 0160–0164). IEEE.
- Lalaoui, L., Mohamadi, T., & Djaalab, A. (2015). New method for image segmentation. *Procedia-Social and Behavioral Sciences*, 195, 1971–1980.
- Li, S., Chen, H., Wang, M., Heidari, A. A., & Mirjalili, S. (2020). Slime mould algorithm: A new method for stochastic optimization. *Future Generation Computer Systems*. doi:10.1016/j.future.2020.03.055.
- Li, C. H., & Lee, C. (1993). Minimum cross entropy thresholding. *Pattern Recognition*, 26(4), 617–625.
- Liang, H., Jia, H., Xing, Z., Ma, J., & Peng, X. (2019). Modified grasshopper algorithm-based multilevel thresholding for color image segmentation. *IEEE Access*, 7, 11258–11295.

- Liu, W., Zhang, Z., Chen, J., Jiang, D., Wu, F., Fan, J., & Li, Y. (2020b). Feasibility evaluation of large-scale underground hydrogen storage in bedded salt rocks of china: A case study in jiangsu province. *Energy*, 1–16. doi:[10.1016/j.energy.2020.117348](https://doi.org/10.1016/j.energy.2020.117348).
- Liu, W., Zhang, Z., Fan, J., Jiang, D., & Daemen, J. (2020c). Research on the stability and treatments of natural gas storage caverns with different shapes in bedded salt rocks. *IEEE Access*, 8, 000507. doi:[10.1109/ACCESS.2020.2967078](https://doi.org/10.1109/ACCESS.2020.2967078).
- Luo, J., Chen, H., Heidari, A. A., Xu, Y., Zhang, Q., & Li, C. (2019). Multi-strategy boosted mutative whale-inspired optimization approaches. *Applied Mathematical Modelling*. doi:[10.1016/j.apm.2019.03.046](https://doi.org/10.1016/j.apm.2019.03.046).
- Mafarja, M., Aljaraah, I., Heidari, A. A., Hammouri, A. I., Faris, H., Ala'M, A.-Z., & Mirjalili, S. (2018). Evolutionary population dynamics and grasshopper optimization approaches for feature selection problems. *Knowledge-Based Systems*, 145, 25–45. doi:[10.1016/j.knosys.2017.12.037](https://doi.org/10.1016/j.knosys.2017.12.037).
- Mirjalili, S. (2016). Sca: A sine cosine algorithm for solving optimization problems. *Knowledge-Based Systems*, 96, 120–133.
- Mirjalili, S., Gandomi, A. H., Mirjalili, S. Z., Saremi, S., Faris, H., & Mirjalili, S. M. (2017). Salp swarm algorithm: A bio-inspired optimizer for engineering design problems. *Advances in Engineering Software*, 114, 163–191.
- Mirjalili, S., & Lewis, A. (2016). The whale optimization algorithm. *Advances in Engineering Software*, 95, 51–67.
- Mirjalili, S., Mirjalili, S. M., & Lewis, A. (2014). Grey wolf optimizer. *Advances in Engineering Software*, 69, 46–61.
- Mohammadi manesh, F., Salehi, B., Mahdianpari, M., Gill, E., & Molinier, M. (2019). A new fully convolutional neural network for semantic segmentation of polarimetric sar imagery in complex land cover ecosystem. *ISPRS Journal of Photogrammetry and Remote Sensing*, 151, 223–236.
- Mousavirad, S. J., & Ebrahimpour-Komleh, H. (2019). Human mental search-based multilevel thresholding for image segmentation. *Applied Soft Computing*.
- Oliva, D., Hinojosa, S., Cuevas, E., Pajares, G., Avalos, O., & Gálvez, J. (2017a). Cross entropy based thresholding for magnetic resonance brain images using crow search algorithm. *Expert Systems with Applications*, 79, 164–180.
- Oliva, D., Hinojosa, S., Osuna-Enciso, V., Cuevas, E., Pérez-Cisneros, M., & Sanchez-Ante, G. (2017b). Image segmentation by minimum cross entropy using evolutionary methods. *Soft Computing*, 1–20.
- Otsu, N. (1979). A threshold selection method from gray-level histograms. *IEEE Transactions on Systems, Man, and Cybernetics*, 9(1), 62–66.
- Pal, N. R., & Pal, S. K. (1993). A review on image segmentation techniques. *Pattern Recognition*, 26(9), 1277–1294.
- Panagiotakis, C., Grinias, I., & Tziritas, G. (2011). Natural image segmentation based on tree equipartition, bayesian flooding and region merging. *IEEE Transactions on Image Processing*, 20(8), 2276–2287.
- Pare, S., Bhandari, A., Kumar, A., & Singh, G. (2019a). Rényi entropy and bat algorithm based color image multilevel thresholding. In *Machine intelligence and signal analysis* (pp. 71–84). Springer.
- Pare, S., Kumar, A., Singh, G., & Bajaj, V. (2019b). Image segmentation using multilevel thresholding: A research review. *Iranian Journal of Science and Technology, Transactions of Electrical Engineering*, 1–29.
- Peng, B., Zhang, L., & Zhang, D. (2013). A survey of graph theoretical approaches to image segmentation. *Pattern Recognition*, 46(3), 1020–1038.
- Ponti, M., Nazaré, T. S., & Thumé, G. S. (2016). Image quantization as a dimensionality reduction procedure in color and texture feature extraction. *Neurocomputing*, 173, 385–396.
- Qiao, W., Huang, K., Azimi, M., & Han, S. (2019a). A novel hybrid prediction model for hourly gas consumption in supply side based on improved whale optimization algorithm and relevance vector machine. *IEEE Access*, 7, 88218–88230. doi:[10.1109/ACCESS.2019.2918156](https://doi.org/10.1109/ACCESS.2019.2918156).
- Rao, R. V., Savsani, V. J., & Vakharia, D. (2011). Teaching–learning-based optimization: A novel method for constrained mechanical design optimization problems. *Computer-Aided Design*, 43(3), 303–315.
- Rashedi, E., Nezamabadi-Pour, H., & Saryazdi, S. (2009). Gsa: A gravitational search algorithm. *Information Sciences*, 179(13), 2232–2248.
- Resma, K. B., & Nair, M. S. (2018). Multilevel thresholding for image segmentation using krill herd optimization algorithm. *Journal of King Saud University-Computer and Information Sciences*.
- Ridha, H. M., Heidari, A. A., Wang, M., & Chen, H. (2020). Boosted mutation-based harris hawks optimizer for parameters identification of single-diode solar cell models. *Energy Conversion and Management*, 209, 112660. doi:[10.1016/j.enconman.2020.112660](https://doi.org/10.1016/j.enconman.2020.112660).
- Saha, C., & Hossain, M. F. (2017). Mri brain tumor images classification using k-means clustering, nsct and svm. In *2017 4th ieee uttar pradesh section international conference on electrical, computer and electronics (upcon)* (pp. 329–333). IEEE.
- Saremi, S., Mirjalili, S., & Lewis, A. (2017). Grasshopper optimisation algorithm: Theory and application. *Advances in Engineering Software*, 105, 30–47.
- Shapiro, L., & Stockman, G. (2001). *Computer vision*. Prentice Hall.
- Shen, L., Chen, H., Yu, Z., Kang, W., Zhang, B., Li, H., ... Liu, D. (2016). Evolving support vector machines using fruit fly optimization for medical data classification. *Knowledge-Based Systems*, 96, 61–75.
- Storn, R., & Price, K. (1997). Differential evolution—a simple and efficient heuristic for global optimization over continuous spaces. *Journal of Global Optimization*, 11(4), 341–359.
- Tang, H., Xu, Y., Lin, A., Heidari, A. A., Wang, M., Chen, H., & Li, C. (2020). Predicting Green Consumption Behaviors of Students Using Efficient Firefly Grey Wolf-Assisted K-Nearest Neighbor Classifiers. *IEEE Access*, 8, 35546–35562.
- Thaher, T., Heidari, A. A., Mafarja, M., Dong, J. S., & Mirjalili, S. (2020). Binary Harris Hawks Optimizer for High-Dimensional, Low Sample Size Feature Selection. *Evolutionary Machine Learning Techniques* (pp. 251–272). Singapore: Springer.
- Unnikrishnan, R., Pantofaru, C., & Hebert, M. (2007). Toward objective evaluation of image segmentation algorithms. *IEEE Transactions on Pattern Analysis and Machine Intelligence*, 29(6), 929–944.
- Vertan, C., Florea, C., Florea, L., & Badea, M.-S. (2017). Reusing the otsu threshold beyond segmentation. In *2017 international symposium on signals, circuits and systems (isscs)* (pp. 1–4). IEEE.
- Wang, M., & Chen, H. (2020). Chaotic multi-swarm whale optimizer boosted support vector machine for medical diagnosis. *Applied Soft Computing*, 88, 105946.
- Wang, M., Chen, H., Yang, B., Zhao, X., Hu, L., Cai, Z., ... Tong, C. (2017). Toward an optimal kernel extreme learning machine using a chaotic moth-flame optimization strategy with applications in medical diagnoses. *Neurocomputing*, 267, 69–84.
- Wang, Z., Bovik, A. C., Sheikh, H. R., Simoncelli, E. P., et al. (2004). Image quality assessment: From error visibility to structural similarity. *IEEE Transactions on Image Processing*, 13(4), 600–612.
- Wilcoxon, F. (1992). Individual comparisons by ranking methods. In *Breakthroughs in statistics* (pp. 196–202). Springer.
- Wolpert, D. H., Macready, W. G., et al. (1997). No free lunch theorems for optimization. *IEEE Transactions on Evolutionary Computation*, 1(1), 67–82.
- Xu, X., & Chen, H. (2014). Adaptive computational chemotaxis based on field in bacterial foraging optimization. *Soft Computing*, 18(4), 797–807.
- Xu, Y., Chen, H., Heidari, A. A., Luo, J., Zhang, Q., Zhao, X., & Li, C. (2019). An efficient chaotic mutative moth-flame-inspired optimizer for global optimization tasks. *Expert Systems with Applications*, 129, 135–155. doi:[10.1016/j.eswa.2019.03.043](https://doi.org/10.1016/j.eswa.2019.03.043).
- Xu, Y., Chen, H., Luo, J., Zhang, Q., Jiao, S., & Zhang, X. (2019). Enhanced Moth-flame optimizer with mutation strategy for global optimization. *Information Sciences*, 492, 181–203.
- Xu, Z., Hu, Z., Heidari, A. A., Wang, M., Zhao, X., Chen, H., & Cai, X. (2020). Orthogonally-designed adapted grasshopper optimization: A comprehensive analysis. *Expert Systems with Applications*, 150, 113282.
- Yang, A. Y., Wright, J., Ma, Y., & Sastry, S. S. (2008). Unsupervised segmentation of natural images via lossy data compression. *Computer Vision and Image Understanding*, 110(2), 212–225.
- Yang, X.-S. (2009). Firefly algorithms for multimodal optimization. In *International symposium on stochastic algorithms* (pp. 169–178). Springer.
- Yang, X.-S. (2010). Firefly algorithm, levy flights and global optimization. In *Research and development in intelligent systems xxvi* (pp. 209–218). Springer.
- Yin, P.-Y. (2007). Multilevel minimum cross entropy threshold selection based on particle swarm optimization. *Applied Mathematics and Computation*, 184(2), 503–513.
- Zhang, Hongliang, Ali Asghar Heidari, Wang, Mingjing, Zhang, Lejun, Chen, Huiling, & Chengye, Li (2020). Orthogonal Nelder-Mead moth flame method for parameters identification of photovoltaic modules. *Energy Conversion and Management*, 211, 112764.
- Zhang, L., Zhang, L., Mou, X., & Zhang, D. (2011). Fsim: A feature similarity index for image quality assessment. *IEEE Transactions on Image Processing*, 20(8), 2378–2386.
- Zhang, X., Xu, Y., Yu, C., Heidari, A. A., Li, S., Chen, H., & Li, C. (2020). Gaussian mutational chaotic fruit fly-built optimization and feature selection. *Expert Systems with Applications*, 141, 112976.
- Zhao, X., Li, D., Yang, B., Ma, C., & Zhu, Y. (2014). *Applied Soft Computing*, 24, 585–596.
- Zhao, X., Li, D., Yang, B., Ma, C., Zhu, Y., & Chen, H. (2014). Feature selection based on improved ant colony optimization for online detection of foreign fiber in cotton. *Applied Soft Computing*, 24, 585–596.
- Zhao, X., Zhang, X., Cai, Z., Tian, X., Wang, X., Huang, Y., ... Hu, L. (2019). Chaos enhanced grey wolf optimization wrapped ELM for diagnosis of paraquat-poisoned patients. *Computational biology and chemistry*, 78, 481–490.
- Zhou, C., Tian, L., Zhao, H., & Zhao, K. (2015). A method of two-dimensional otsu image threshold segmentation based on improved firefly algorithm. *2015 ieee international conference on cyber technology in automation, control, and intelligent systems (cyber)* (pp. 1420–1424). IEEE.
- Zhu, W., Ma, C., Zhao, X., Wang, M., Heidari, A. A., Chen, H., & Li, C. (2020). Evaluation of Sino Foreign Cooperative Education Project Using Orthogonal Sine Cosine Optimized Kernel Extreme Learning Machine (8, pp. 61107–61123). IEEE Access. doi:[10.1109/ACCESS.2020.2981968](https://doi.org/10.1109/ACCESS.2020.2981968).